

Stony Brook University



OFFICIAL COPY

The official electronic file of this thesis or dissertation is maintained by the University Libraries on behalf of The Graduate School at Stony Brook University.

© All Rights Reserved by Author.

Design, Synthesis and Evaluation of Inhibitors of the enoyl-ACP reductase from
Staphylococcus aureus and *Yersinia pestis*

A Thesis Presented

by

Sonam Shah

to

The Graduate School

in Partial Fulfillment of the

Requirements

for the Degree of

Master of Science

in

Chemistry

Stony Brook University

August 2012

Stony Brook University

The Graduate School

Sonam Shah

We, the thesis committee for the above candidate for the
Master of Science degree, hereby recommend
acceptance of this thesis.

**Peter J. Tonge, Ph.D. – Thesis Advisor
Professor, Department of Chemistry**

**Iwao Ojima, Ph.D. – Chairperson of Defense
Distinguished Professor, Department of Chemistry**

**Dale G. Drueckhammer, Ph.D. – Third member of Defense
Professor, Department of Chemistry**

This thesis is accepted by the Graduate School

Charles Taber
Interim Dean of the Graduate School

Abstract of the Thesis

Design, Synthesis and Evaluation of Inhibitors of the enoyl-ACP reductase in

Staphylococcus aureus and *Yesinia pestis*

by

Sonam Shah

Master of Science

in

Chemistry

Stony Brook University

2012

Infectious diseases, caused by pathogenic biological agents, are the leading causes of death worldwide, especially in low-income countries. Two such pathogenic bacteria that are our centers of interest are *Staphylococcus aureus*, the most common cause of hospital acquired infection and *Yesinia pestis*, the priority pathogen that causes plague. In order to develop drugs against these pathogens, we focus on the fatty acid biosynthesis (FASII) pathway, a validated target for drug discovery due to structural differences between eukaryotic and prokaryotic fatty acid synthesis machinery. Previously, a library of diphenyl ethers synthesized by our lab exhibited potent inhibition of the enzyme enoyl-ACP reductase (FabI) that catalyzes the rate limiting step of fatty acid biosynthesis in these pathogens. Although, these inhibitors showed *in vivo* activity, we wanted to develop alternative inhibitors that are metabolically more stable.

Thus, we synthesized a novel library of 2-pyridones inhibitors that are metabolically stable and are also hypothesized to have similar binding interaction with FabI as the diphenyl ethers. In this thesis, we report the synthesis and preliminary inhibition data for 2-pyridones as novel inhibitors of saFabI and ypFabV, the enoyl-ACP reductases from *S. aureus* and *Y. pestis*, respectively.

Table of Contents

Abstract of the Thesis	iii
Table of Contents	v
List of Figures	vii
List of Schemes	viii
List of Tables	ix
List of Abbreviations	x
Acknowledgments	xiv
Chapter 1: Introduction	1
The history of antibiotics	1
Mechanism of drug resistance	2
Treatment	3
FASII pathway: Novel drug target	4
Enoyl-ACP reductase	6
Inhibition of FabI	7
FabI inhibitors that covalently modify the inhibitor	8
Non-covalent inhibitors of enoyl-ACP reductase	9
Research Project Overview	12
Chapter 2: SAR of novel 2-pyridone inhibitors against <i>Staphylococcus aureus</i> enoyl-ACP reductase	13
Background	13
Design and synthesis of novel 2-pyridone	15
Results and Discussion	15
Chemistry	15
Discussion	19
SAR Analysis	23
B-ring mono-substituents:	24
A-ring analysis:	26
Conclusion	27
Chapter 3: Inhibition of <i>Yesinia pestis</i> enoyl-ACP reductase by the 2-pyridones	29

Enoyl ACP reductase FabV	30
Project goal	31
Results and Discussion.....	32
SAR data analysis	37
Conclusion.....	39
Chapter 4: Novel diphenyl ethers and mechanistic studies of InhA.....	40
Background	40
Slow onset inhibition.....	42
Results and Discussion.....	45
Slow-onset inhibitors of InhA	45
Synthesis PT163:	47
Discussion.....	47
Conclusion.....	49
Chapter 5: Future work	50
Inhibition studies of 2-pyridone inhibitors against other pathogens	50
Future direction	56
Chapter 6: Materials and methods	57
General procedures for compound synthesis:	57
Compound Characterization.....	60
Measurement of IC ₅₀	72
Synthesis of trans-2-Dodecenoyl-CoA (DDCoA).....	73
Expression and Purification of enzymes	73
References.....	74

List of Figures

Figure 1. History of Antibiotics (6)	2
Figure 2. Key steps in the genomics-driven antibiotic drug discovery process (8).....	4
Figure 3. Fatty acid biosynthesis pathway in <i>E. coli</i> (5).....	5
Figure 4. Proposed mechanism of <i>E. coli</i> FabI (6).....	7
Figure 5. Diazaborine inhibitor of <i>E. coli</i> FabI.....	8
Figure 6. Mechanism of action of INH.....	9
Figure 7. Structure of triclosan 2, non-covalent inhibitor of enoyl ACP-reductase	10
Figure 8. Triclosan bound to <i>E. coli</i> FabI (26).	10
Figure 9. Potent diphenyl ether inhibitor of InhA	11
Figure 10. 2-pyridone inhibitor, CG400549 in phase I clinical trial	11
Figure 11. Diphenyl ether inhibitors of <i>Staphylococcus aureus</i>	14
Figure 12. saFabI bound to Triclosan (33)	14
Figure 13. Triclosan bound to saFabI (33).	17
Figure 14. Residues in the active site of saFabI (33).....	24
Figure 15. Comparison between the two classes of 2-pyridone inhibitors with the natural substrate of FabI.	27
Figure 16. Overlap of ypFabV without inhibitor (light green) and ypFabV (light blue) bound to PT173 (48).....	33
Figure 17. Interactions between PT173 (shown in cyan) with ypFabV residues.	34
Figure 18. Cell wall of <i>Mycobacterium tuberculosis</i> (52).....	42
Figure 19. Energy profile for slow-onset inhibition.	44
Figure 20. Diphenyl ether inhibitors of InhA.	45
Figure 21. Structure of PT70 bound to InhA.....	46
Figure 22. Interactions of PT70 with InhA.....	48

List of Schemes

Scheme 1. Synthesis of 2-pyridone inhibitors.	16
Scheme 2. Synthesis of the bromo-compounds.....	16
Scheme 3. Synthesis of 2-pyridones with bridging oxygen.....	18
Scheme 4. Synthesis of compound 3.	19
Scheme 5. Synthesis of PT163.	46

List of Tables

Table 1. Inhibition of saFabI by the 2-pyridone inhibitors.....	21
Table 2. Inhibition of ypFabV by the 2-pyridone inhibitors.....	35
Table 3. Binding kinetics of diphenyl ethers	49
Table 4. Inhibition of InhA by the 2-pyridone inhibitors.	50
Table 5. Inhibition of ftuFabI by the 2-pyridone inhibitors.....	52
Table 6. Inhibition of bpmFabI by the 2-pyridone inhibitors	53

List of Abbreviations

°C	degree centigrade
µg	microgram
AcAc-CoA	Acetoacetyl-CoA
AccABCD	Acetyl-CoA carboxylase
ADMET	Absorption Distribution Metabolism Excretion and Toxicity
<i>B.pseudomallei</i>	<i>Burkholderia pseudomallei</i>
bpmFabI	Enoyl-ACP reductase from <i>Burkholderia pseudomallei</i>
CH ₂ Cl ₂	Dichloromethane
clogP	Calculated logarithm of partition coefficient between n-octanol and water
CoA	Coenzyme A
d	doublet
DD-CoA	<i>trans</i> -2-Dodecenoyl-CoA
DMSO	Dimethyl sulfoxide
DMPK	Drug metabolism pharmacokinetics
<i>E. coli</i>	<i>Escherichia coli</i>
ecFabI	Enoyl-ACP reductase from <i>Escherichia coli</i>
ESI-MS	Electrospray mass spectrometry

EtOAc	Ethyl-acetate
EtOH	Ethanol
<i>F. tularensis</i>	<i>Francisella tularensis</i>
FabI	Enoyl-ACP reductase
FabK	Enoyl-ACP reductase
FabL	Enoyl-ACP reductase
FabV	Enoyl-ACP reductase
FAS-I	Eukaryotic fatty acid biosynthesis
FAS-II	Bacterial fatty acid biosynthesis
HTS	High-throughput screening
IC ₅₀	Half maximal inhibitory concentration
INH	Isoniazid
InhA	Enoyl-ACP reductase from <i>Mycobacterium tuberculosis</i>
J	Coupling constant (NMR)
K	Equilibrium constant
k _{on}	Association rate-constant
k _{off}	Dissociation rate-constant
KatG	Mycobacterial catalase peroxidase
m	Multiplet
<i>M. tuberculosis</i>	<i>Mycobacterium tuberculosis</i>
MDR-TB	Multidrug resistant TB
MIC	Minimum inhibitory concentration

mg	Milligram
min	Minutes
mL	Milliliter
MS	Mass Spectrum
MTB	<i>Mycobacterium tuberculosis</i>
NAD ⁺	Nicotinamide adenine dinucleotide (oxidized)
NADH	Nicotinamide adenine dinucleotide (reduced)
NADP ⁺	Nicotinamide adenine dinucleotide phosphate (oxidized)
NADPH	Nicotinamide adenine dinucleotide phosphate (reduced)
nM	Nanomolar
NMR	Nuclear Magnetic Resonance
pdb	Protein data bank
pfFabI	Enoyl-ACP reductase from <i>Plasmodium falciparum</i>
rt	Room temperature
s	Singlet
<i>S. aureus</i>	<i>Staphylococcus aureus</i>
saFabI	Enoyl-ACP reductase from <i>Staphylococcus aureus</i>
SAR	Structure Activity Relationship
SDR	Short chain dehydrogenase/reductase

t	Triplet
TB	Tuberculosis
THF	Tetrahydrofuran
<i>V. cholerae</i>	<i>Vibrio cholerae</i>
WHO	World Health Organization
WT	Wild-type
XDR	Extensively-drug resistant
<i>Y. pestis</i>	<i>Yersinia pestis</i>
ypFabV	Enoyl-ACP reductase from <i>Yersinia pestis</i>

Acknowledgments

First and foremost I would like to express my heartfelt thanks to my advisor Professor Peter J. Tonge for giving me a wonderful opportunity to work in his research group and for his continuous encouragement, constant support and invaluable guidance throughout my research work at Stony Brook University. I am also grateful to Professor Ojima and Professor Drueckhammer for being my committee members and for their noteworthy advice.

A special thanks to all the Tonge group members for making my stay in the lab one of the most cherished moments of my life. Thank you all for providing me a dynamic environment for both work and fun. My heartfelt gratitude towards my mentor, Dr. Gopal R. Bommineni for teaching me various techniques in Organic Chemistry and helping me in my project.

Last but not the least, I would like to thank the Almighty God, my parents and my friends for their help, guidance and encouragement.

Chapter 1: Introduction

The history of antibiotics

Infectious diseases are a major cause of concern worldwide. Natural products have been used for curing diseases throughout the history of mankind. In the latter part of the nineteenth century, different substances were identified that inhibited bacterial growth. In 1877, Louis Pasteur and Robert Koch observed that an airborne bacillus inhibited the growth of the pathogen *Bacillus anthracis* (1). In late 1880s, Paul Ehrlich discovered a synthetic compound Salvarsan for the treatment of syphilis (2). The Nobel Prize winning serendipitous discovery of the antibiotic penicillin by Alexander Fleming in the year 1928 followed this (3). Around the same time, in 1932, Gerhard Domagk who won the Nobel Prize for medicine in 1939 developed the sulfonamide drug Prontosil. The discovery of penicillin and sulfonamide drugs gave rise to the “golden era” in medicine (4). Figure 1 shows the various antibiotics introduced since the 1900s. The introduction of these drugs in addition to streptomycin greatly reduced the mortality by infectious diseases. Thus, the drug discovery research slowed down and no new class of antibiotics was introduced from 1960 till 2000 (5, 6). However, adaptation to natural selection led to the emergence of drug resistant strains of various pathogens. Presently in the US and UK, 40-60% of the cases reported for *S. aureus* infection are MRSA (methicillin resistant staphylococcus aureus) or multidrug resistant (MDR) strains (7). Similarly, TB reemerged in

immune-compromised patients infected by HIV. This is followed by XDR (extremely drug-resistant) strains that are untreatable with the first generation drugs.

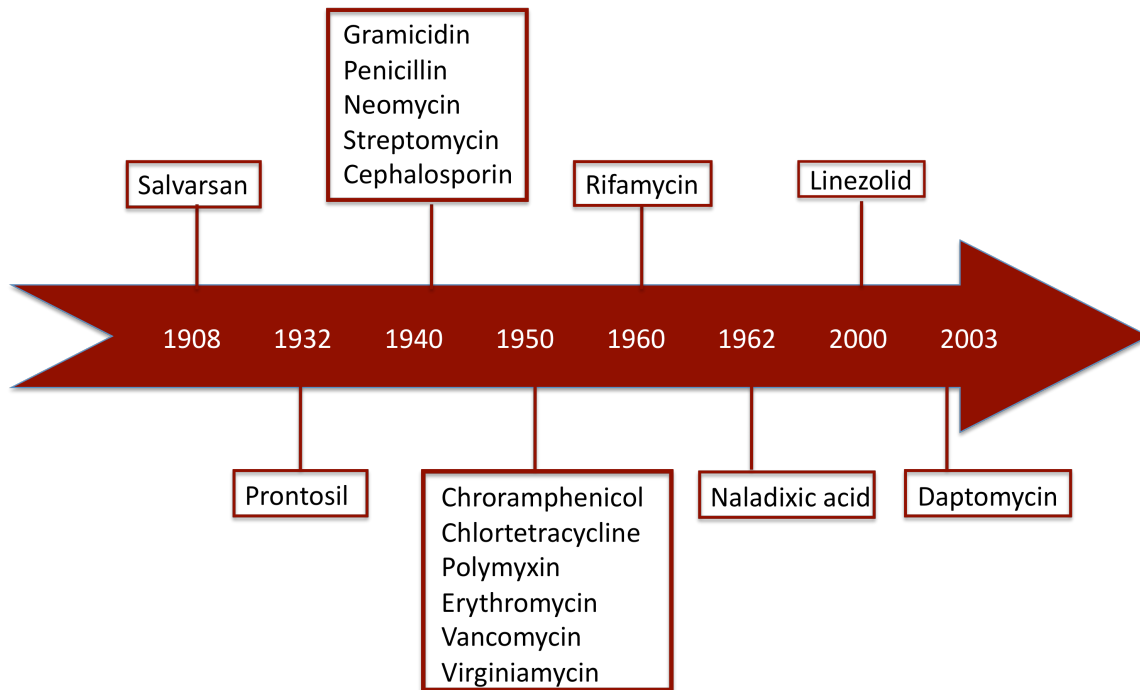


Figure 1. History of Antibiotics [figure modified from (6)]

Mechanism of drug resistance

There are two main components of drug resistance problem: a) The antibiotic that inhibits the susceptible micro-organism and selects the resistant ones; b) The genetic resistant determinant in micro-organism selected by the antibiotic drug (7). Drug resistance occurs when these two factors come together in the host or in the environment. This problem is aggravated and extended when the host under continued antimicrobial selection spreads the selected resistance gene.

Drug resistance of a pathogen can be intrinsic or can be acquired after being exposed to antibiotics. There are various mechanisms by which drug resistance occurs (7):

1. Degradation of the antibiotic by the enzyme, for example, destruction of penicillin by β -lactamase enzymes.
2. Intracellular target site is modified due to which the drug does not inhibit the target with high affinity.
3. Efflux pump over expression causing the removal of the antibiotic from the bacterial cell, for example, tetracyclines and chloramphenicol.
4. Modification in the cell wall structure thereby preventing the permeability of the antibiotic.

It is important to note that more than one kind of mechanism can occur simultaneously thereby contributing to drug resistance.

Treatment

One of the methods for the treatment of drug resistant strains is identification of novel molecular targets essential for the growth of the pathogen. The screening of compound libraries for whole cell activity can lead to the identification of lead compound for drug-discovery. Alternatively, genetic methods can be employed to identify putative targets that then can be subject to rational inhibitor discovery. Once a lead compound is identified, further optimization is often required that employs SAR studies to enhance the inhibition properties. These *ex-vivo*

studies are followed by pharmacokinetic and pharmacodynamic studies in animal infection models and finally progression into clinical trials. This is shown schematically in Figure 2.

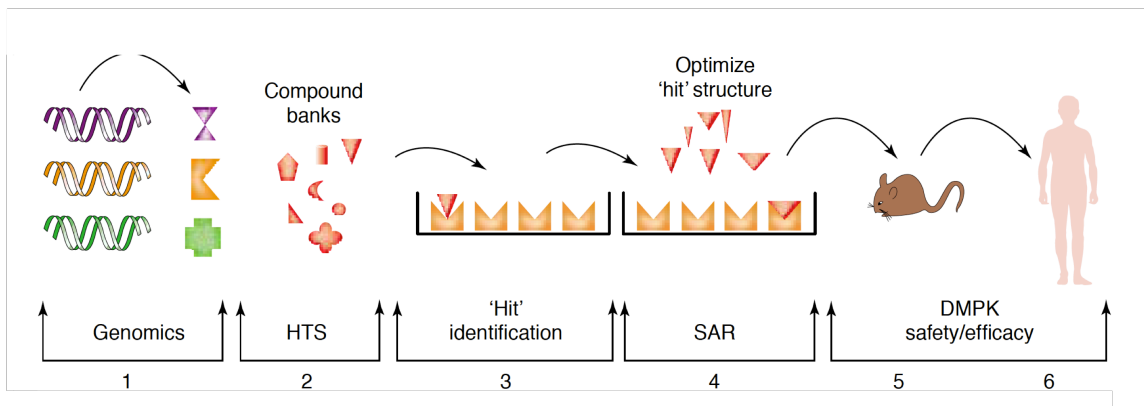


Figure 2. Key steps in the genomics-driven antibiotic drug discovery process (8)

HTS: High throughput screening; SAR: Structure-Activity Relationship; DMPK: Drug metabolism and Pharmacokinetics

FASII pathway: Novel drug target

The type II fatty acid biosynthesis pathway (FASII) present in prokaryotes is a novel and relatively unexplored target for drug discovery. Gene-knockdown and knockout experiments show that this pathway is essential for the survival of the pathogen (8-10).

Fatty acids are essential for the survival of all organisms. Fatty acid are the precursors of phospholipids and in bacteria, fatty acids are essential components of cell wall. It has been shown previously that the inhibition of FASII pathway in bacteria causes the disruption of cell wall and cell membrane (11, 12). Fatty acid synthesis (FAS) can be divided into two types depending on the basic architecture of the enzymes involved - FASI and FASII. In FASI pathway, which is usually found in eukaryotes, a single gene encodes a multifunctional

polypeptide that carries out all the elongation steps. Conversely, in FASII, each step is catalyzed by a unique mono-functional peptide. This type of fatty acid biosynthesis is usually present in bacteria, plants and parasites. The architectural difference between human FAS (FASI) and bacterial FAS (FASII) makes the enzymes in FASII potential drug targets. Figure 3 shows FASII pathway in *E.coli*.

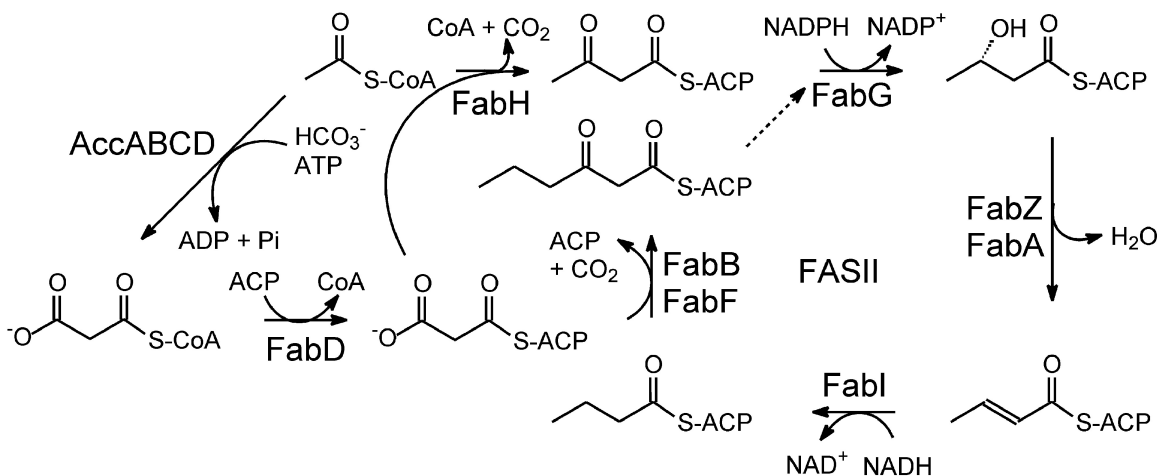


Figure 3. Fatty acid biosynthesis pathway in *E. coli* (5).

AccABCD: acetyl-CoA carboxylase; FabD: malonyl-CoA:ACP transacylase; FabG: β -ketoacyl reductase; FabA/FabZ: β -hydroxyacyl dehydrase; FabI: enoyl reductase. FabH: β -ketoacyl synthase III initiates condensation reaction; FabB/FabF: β -ketoacyl synthase I and II: responsible for further elongation rounds.

Enzymes of the FAS-II pathway can be divided into two sets of enzymes encoded by separate genes. The first group of enzymes is responsible for the initiation of fatty acid biosynthesis. Here, acetyl-CoA carboxylase (ACC) converts acetyl-CoA to malonyl-CoA. This step requires the co-ordination of four gene products AccA, AccB, AccC and AccD. Once malonyl-CoA is formed, malonyl-CoA:ACP transacylase enzyme, FabD, transfers the malonyl moiety to the terminal sulphhydryl of ACP (acyl carrier protein). It is important to note that the

intermediates in the FAS pathway shuttle between enzymes with the help of ACP. Thus, this protein cofactor is a partner in all the subsequent reactions. The second enzyme β -ketoacyl ACP synthase-III, FabH, catalyzes the condensation of acetyl CoA and malonyl ACP forming acetoacetyl ACP.

Acetoacetyl-ACP initiates the second module of elongation. β -Ketoacyl ACP reductase (FabG) reduces the C3 carbonyl to a hydroxyl group using NADPH as the cofactor (13, 14). This intermediate is then dehydrated by β -hydroxyacyl ACP dehydratases (FabA or FabZ) forming β -hydroxyacyl-ACP. The last step of the elongation cycle is the reduction of the C2-C3 double bond in the presence of NADH cofactor by the enoyl-ACP reductase (FabI). Thus, in each elongation cycle two carbons are added to the growing acyl-chain.

Enoyl-ACP reductase

As shown in Figure 4, the enoyl-ACP reductase is involved in the reduction of the double bond in the last step of the elongation cycle of the fatty acid biosynthesis in prokaryotes. This step is the slowest step in the fatty acid biosynthesis pathway and is important for the viability of the bacteria (15). This enzyme has four isoforms, FabI, FabV, FabK and FabL, which with the exception of FabK, belong to the short chain dehydrogenase (SDR) family. Members of the SDR family have a highly conserved Tyr-(X)₆-Lys motif. FabV from *Vibrio cholera* is 60% larger than FabI and has a Tyr-(X)₈-Lys motif. FabL from *Bacillus subtilis* uses NADPH as the cofactor

while saFabI uses NADPH as the cofactor because it has a charged binding pocket for the ribose phosphate. The proposed mechanism of reduction by the enoyl-ACP reductase involves the transfer of hydride from the cofactor NAD(P)H to the C3 position of the C2-C3 double bond leading to the formation of an enolate ion. The active site Tyr donates the proton to the C2 carbonyl. The Tyr residue then accepts the proton from the proton chain involving the hydroxyl group of the ribose of the cofactor, NAD(P)H, and the side chain amine of the active site Lys residue, and four water molecules that communicate with the bulk solvent.

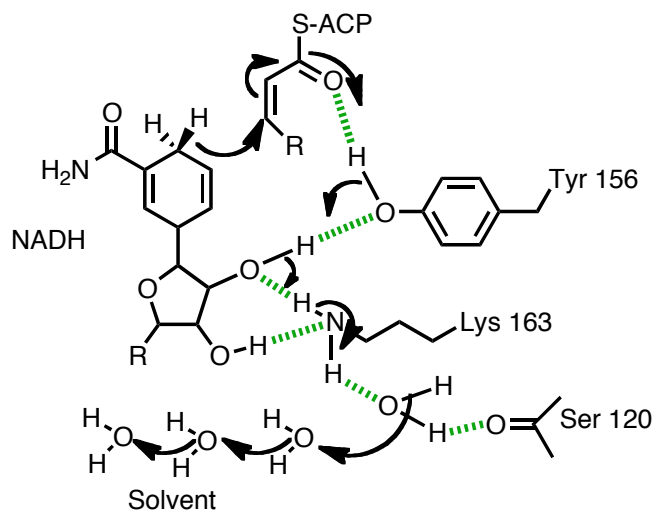


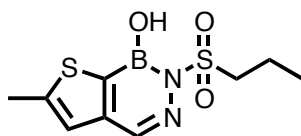
Figure 4. Proposed mechanism of *E. coli* FabI [figure modified from (6)]

Inhibition of FabI

Inhibitors of FabI can be divided into two classes- those that form a covalent adduct with the cofactor and those that bind non-covalently to the enzyme complex (5).

FabI inhibitors that covalently modify the inhibitor

Diazaborines contain a boron atom that forms a covalent bond with the 2'-hydroxyl group of the NAD⁺. These inhibitors form π - π stacking interactions with the NAD⁺ and Van der Waals interactions in the substrate-binding pocket. The diazaborine binds to NAD⁺ in the active site where the substrate is located. Therefore, these are bisubstrate inhibitors of FabI (16). Mechanistic studies have shown that the diaza-moiety and the boron atom are essential for inhibition (17, 18). Figure 5 shows a potent diazaborine inhibitor **1** of *E. coli* with an MIC of 1.25 $\mu\text{g/mL}$ (17). The diazaborines are found to inhibit the FAS in *E. coli* and not in FAS in eukaryotes.



MIC = 1.25 $\mu\text{g/mL}$

1

Figure 5. Diazaborine inhibitor of *E. coli* FabI

Isoniazid (INH) is one of the frontline drugs for the treatment of tuberculosis. This drug was introduced in 1952 but it was not until 1994 that the target of the drug was identified. *InhA* gene in *Mycobacterium tuberculosis* (MTB) encodes for InhA, the FabI in MTB, was found to be the target for INH (19). INH is a pro drug that requires activation by the catalase peroxidase enzyme KatG (20). The activated form of the drug forms a covalent bond with the cofactor

NADH that leads to inhibition of InhA. Figure 6 shows the INH-NAD adduct that is a bi-substrate inhibitor of InhA. Mutations in KatG have been shown to result in resistance to INH (21).

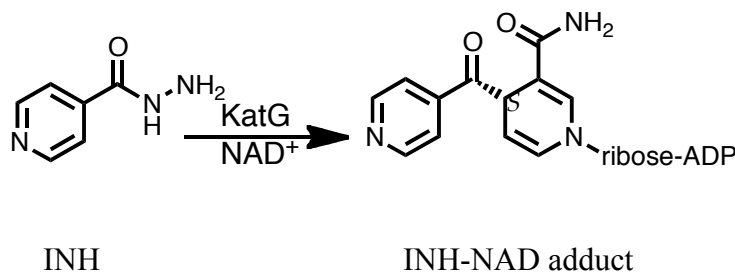
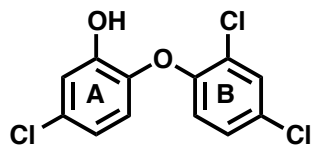


Figure 6. Mechanism of action of INH. INH is activated by KatG which reacts with NAD^+ forming the INH-NAD adduct

Non-covalent inhibitors of enoyl-ACP reductase

Triclosan **2**, (Figure 7), a diphenyl ether that is present as an antibacterial agent in many consumer products blocked the lipid biosynthesis in *E. coli*, *S. aureus*, *P. falciparum* and *M. tuberculosis*. Further research revealed that triclosan inhibits the FabI enzyme in *E. coli* with an equilibrium binding constant (K_i) of 7 pM (22), InhA with $K_i = 200$ nM (23, 24), saFabI with $K_i = 5$ nM (5) and pfFabI with $\text{IC}_{50} = 73$ nM (25). The phenolic ring of triclosan forms a π - π stacking interaction with the NAD^+ , while the other aromatic ring is perpendicular to the phenolic ring. Figure 8 shows the structure of triclosan bound to ecFabI. Binding of triclosan leads to the ordering of the substrate-binding loop (26) (shown in magenta). This has been proposed to be the slow step in the formation of the final enzyme-inhibitor complexes.



Triclosan

2

Figure 7. Structure of triclosan 2, non-covalent inhibitor of enoyl ACP-reductase

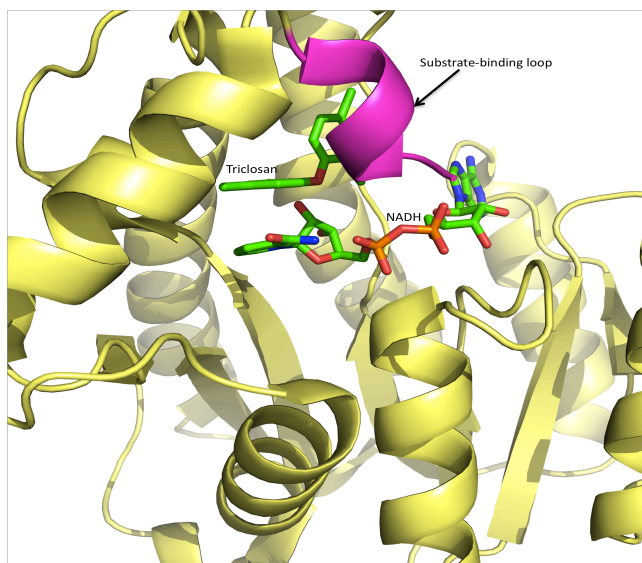
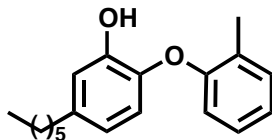


Figure 8. Triclosan bound to *E. coli* FabI.

The ordered substrate-binding loop is shown in magenta (26).

Extensive SAR studies have been performed to explore the essential features of the diphenyl ether scaffold of triclosan that are important for interaction with FabI from different pathogens. In the course of these studies, our lab has developed a series of diphenyl ethers that significantly inhibit the FabI enzymes from pathogens including *E. coli*, *S. aureus*, *F. tularensis*

and *M. tuberculosis*. Figure 9 shows one such potent inhibitor, **PT70**, which is a slow tight binding inhibitor of InhA (27).

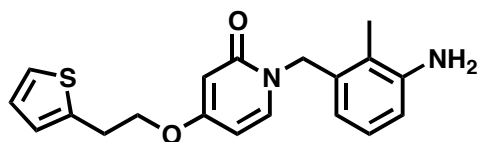


PT70

$K_i = 22 \text{ pM}$, $\text{MIC} = 3 \text{ } \mu\text{g/mL}$

Figure 9. Potent diphenyl ether inhibitor of InhA

Although these diphenyl ethers are potent inhibitors, the phenolic hydroxyl is liable to Phase II metabolism reaction as these are hydrophobic molecules (28). Hence in order to improve the ADMET (Absorption Distribution Metabolism Excretion and Toxicity) properties of the inhibitor we adopted the 2-pyridone scaffold that is metabolically more stable. Moreover, the 2-pyridone inhibitor **3**, CG400549, of *S. aureus* FabI is in Phase I clinical trial (Figure 10) (29).



3

Figure 10. 2-pyridone inhibitor, CG400549 in phase I clinical trial

Research Project Overview

Based on our knowledge that diphenyl ether inhibitors are metabolically unstable, we designed and synthesized a library of 2-pyridone inhibitors and tested it against the enoyl-ACP reductases of various pathogens, in particular, saFabI and ypFabV.

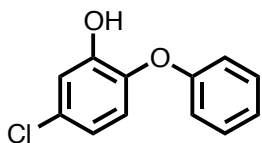
Chapter 2: SAR of novel 2-pyridone inhibitors against *Staphylococcus aureus* enoyl-ACP reductase

Background

Staphylococcus aureus was first discovered in 1880 in Scotland (30). It is a gram-positive bacteria. The literal meaning of *S. aureus* is “golden cluster seeds”. This bacterium appears as short-chains or grape like under the microscope. According to the WHO report in 1998, about one third of the world population is infected by *S. aureus*. This bacteria is usually present on the skin and anterior nares from where it can enter the body and cause further infection. *S. aureus* can cause minor skin infections like skin lesion to major infections like arthritis and pneumonia. It is one of the major causes of nosocomial infection when the bacteria is transferred from the body of the health worker to the patient via skin contact or may be due to post-surgical skin infection.

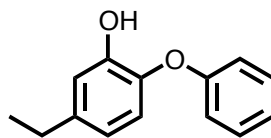
Triclosan also inhibits the fatty acid biosynthesis in *Staphylococcus aureus*. The emergence of drug resistant strains of this bacteria such as methicillin resistant *S. aureus* (MRSA) and vancomycin resistant *S. aureus* (VRSA) are presently a great cause of concern. Inhibition studies show that triclosan inhibits saFabI with $K_i = 5$ nM (5). Previously, it has been reported that triclosan also inhibits the growth of MRSA (31, 32). Based on the diphenyl ethers

scaffold of triclosan, two compounds EPP and CPP (Figure 11) were found to have K_i values of 5-9 nM. Furthermore, these are slow onset inhibitors of saFabI. Figure 12 shows the structure of triclosan bound to saFabI.



CPP

$K_i = 2$ nM, MIC = 0.06 $\mu\text{g/mL}$



EPP

$K_i = 8$ nM, MIC = 0.03 $\mu\text{g/mL}$

Figure 11. Diphenyl ether inhibitors of *Staphylococcus aureus*

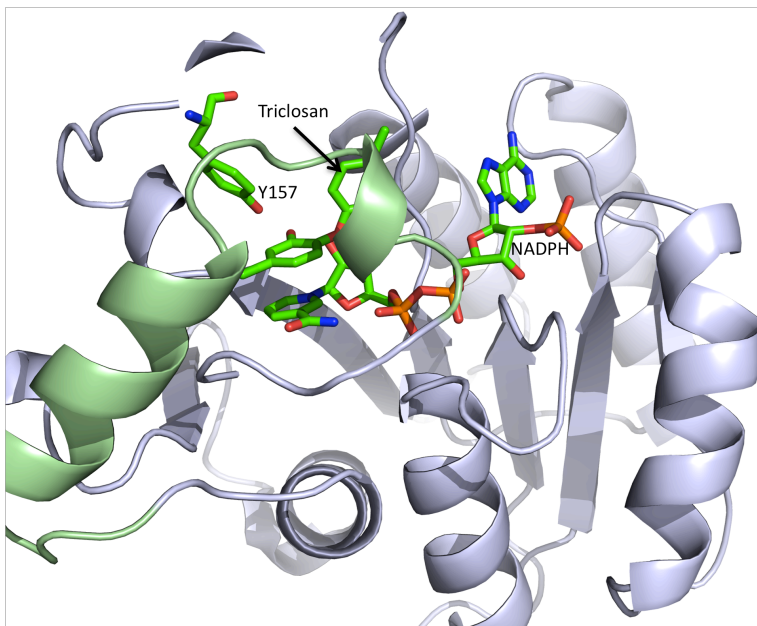


Figure 12. saFabI bound to Triclosan.

Substrate-binding loop is shown in green. Y157, the active site residue is also shown (33)

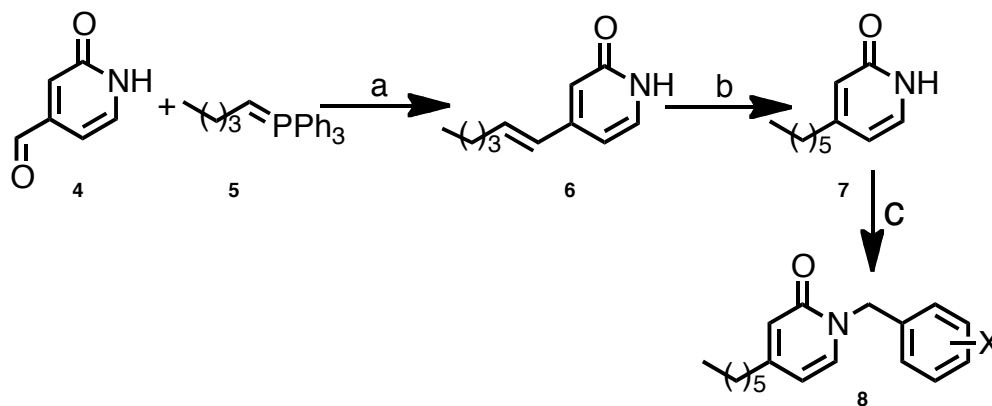
Design and synthesis of novel 2-pyridone

Docking experiments have shown that 2-pyridones, a novel class of inhibitors, could replace the A ring of triclosan. As shown in Chapter 3, the 2-pyridone scaffold retains the essential structural features like π - π stacking interactions with NAD^+ and phenolic H-bonding interactions. The 2-pyridone compounds have been found to inhibit FabI of the pathogen *Bacillus anthracis* (34). Also as stated above, the 2-pyridone derivative **3**, (shown in Chapter 1) is in Phase I clinical trials for the treatment of *S. aureus* infection. Based on the above information we designed novel 2-pyridone inhibitors against saFabI.

Results and Discussion

Chemistry

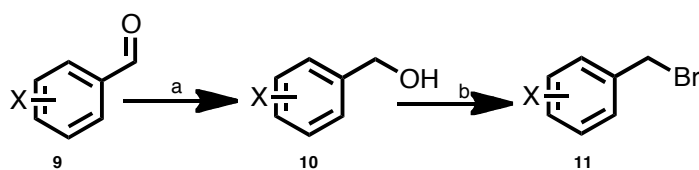
The preparation of the 2-pyridones is shown in **Scheme 1**. The first step was the Wittig reaction between aldehyde **4** and n-pentyl triphenyl phosphine bromide **5** in the presence of the base n-BuLi at -78°C . This was followed by catalytic reduction of **6** to give the intermediate **7**. Compound **7** was then treated with different alkyl bromides in the presence of K_2CO_3 at 80°C for 5h leading to the formation of the final compounds **8**.



Scheme 1. Synthesis of 2-pyridone inhibitors.

Reagents and conditions: (a) *n*-BuLi, THF, -78 °C; (b) H₂, MeOH, rt; (c) K₂CO₃, CH₃CN, 80 °C, X-ArCH₂Br

If the bromide for the final reaction was commercially unavailable, it was synthesized as shown in **Scheme 2**. The corresponding aldehyde **9** was reduced using NaBH₄ to form the primary alcohol **10**. This alcohol then undergoes substitution reactions in the presence of PBr₃ to form the bromo-compound **11**. Both these reactions are clean and do not require purification.



Scheme 2. Synthesis of the bromo-compounds

Reagents and conditions: (a) NaBH₄, MeOH, rt (b) PBr₃, Et₂O, rt

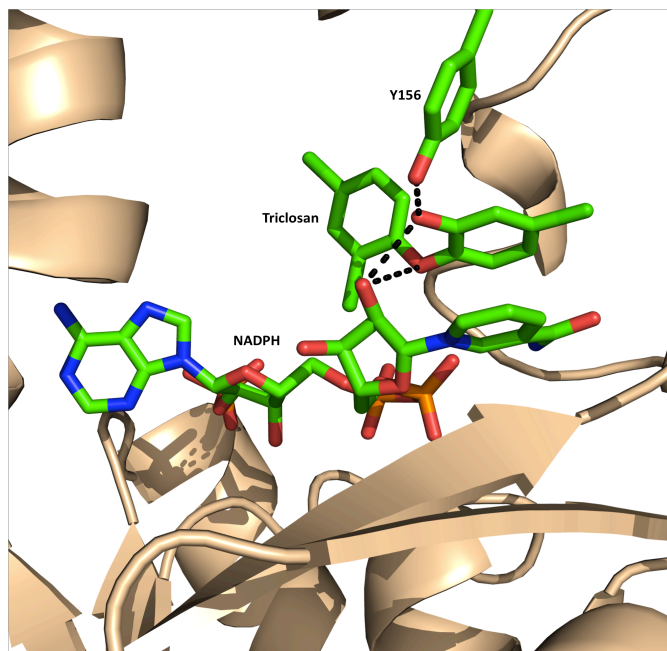
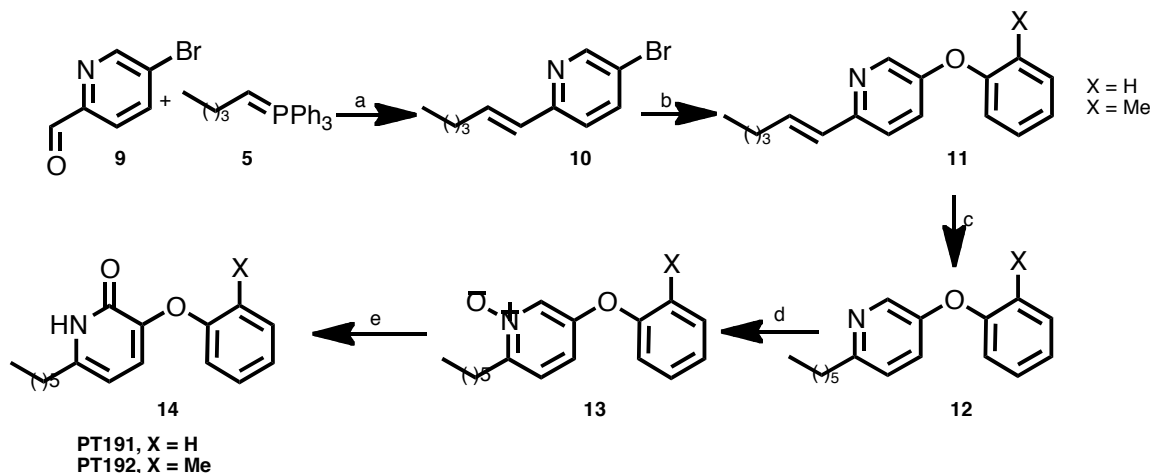


Figure 13. Triclosan bound to saFabI.

In black are shown the H-bonds between -OH of Y156, -OH and bridging O of triclosan and NADPH (33).

Unlike diphenyl ethers, the 2-pyridones do not have bridging oxygen. The crystal structure of the diphenyl ether triclosan bound to saFabI shows that the bridging oxygen of diphenyl ether forms H-bond to 2'-OH of NAD⁺ as shown in Figure 13. Assuming that 2-pyridones bind similar to diphenyl ethers, this interaction is potentially absent in the 2-pyridones that we synthesized. Thus, in order to study the effect of the bridging oxygen, we synthesized **PT191** and **PT192** that are 2-pyridone structures with bridging oxygen.

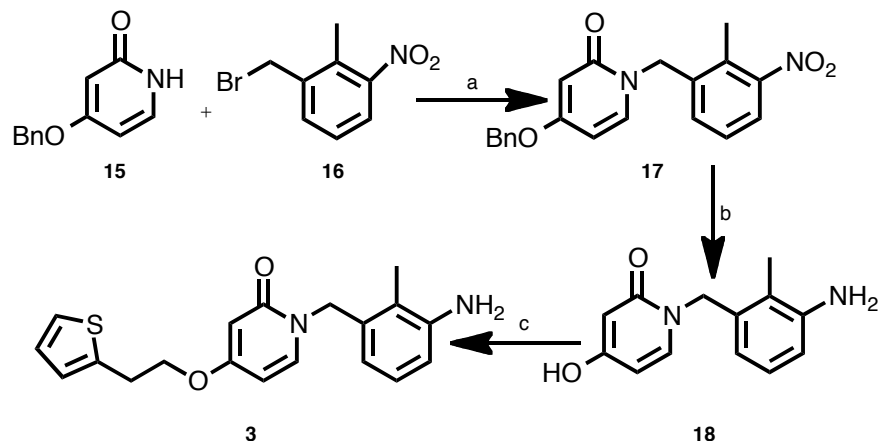


Scheme 3. Synthesis of 2-pyridones with bridging oxygen.

Reagents and conditions: (a) n-BuLi, THF, -78 °C; (b) ArOH picolinic acid, CuI, K₃PO₄, DMSO 90 °C; (c) H₂, Pd/C, MeOH, rt; (d) mcpba, CHCl₃, rt; (e) (i) Ac₂O, reflux; (ii) HCl, 90 °C

The synthesis of compound **PT191** and **PT192** is shown in **Scheme 3**. Commercially available **9** is reacted with n-pentyl triphenyl phosphine bromide **5** under Wittig reaction conditions to form compound **10**. This is then coupled with the corresponding phenol to form compound **11**. The side chain of compound **11** is reduced by catalytic hydrogenation forming compound **12**. Compound **12** is then oxidized in the presence of MCPBA leading to the formation of compound **13** that finally undergoes rearrangement in the presence of Ac₂O followed by HCl forming compound **14**.

In order to compare the potency of our compounds, we also synthesized compound **3**, CG400549 as shown in **Scheme 4**.



Scheme 4. Synthesis of compound 3.

(a) K_2CO_3 , CH_3CN , $80\text{ }^\circ\text{C}$; (b) H_2 , Pd/C , MeOH , rt ; (c) Cs_2CO_3 , NaI , DMF , rt

Commercially available **15** undergoes substitution reaction with corresponding bromide **16** forming compound **17**. Catalytic reduction of **17** leads to reduction of nitro to amine and debenylation forming compound **18**. Compound **18** then undergoes substitution reaction in the presence of Cs_2CO_3 and NaI forming the final compound **3**.

Discussion

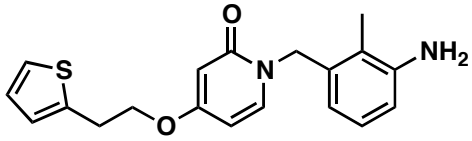
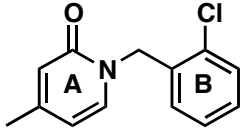
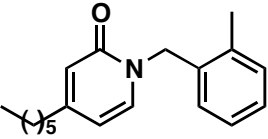
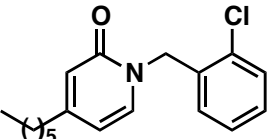
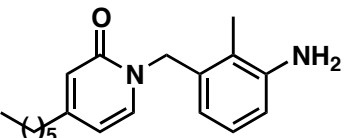
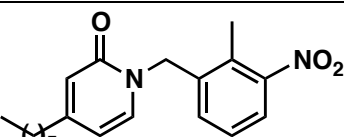
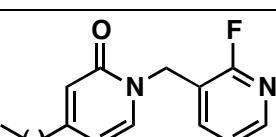
The bioavailability of a compound *in vivo* is one of the major hurdles in the development of novel drugs. Bioavailability is defined as the fraction of drug that reaches the systemic circulation compared to the total administered drug dose (35). When a drug is administered orally, there are xenobiotic mechanisms that lead to metabolic degradation of the drug. Hence, bioavailability of a drug is an important concept for designing novel drug molecules.

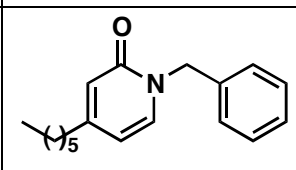
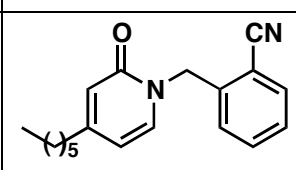
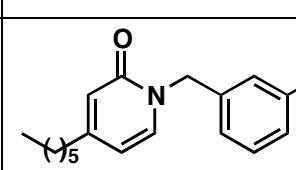
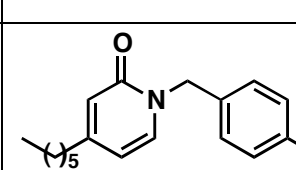
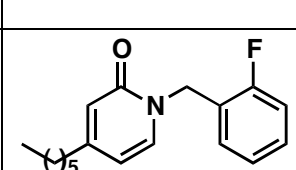
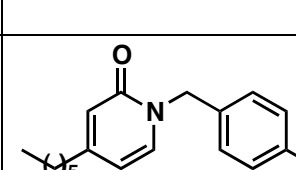
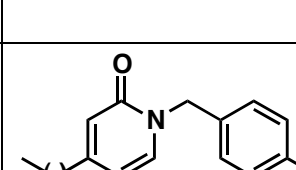
Lipinski *et al* outlined a set of parameters to assess the oral bioavailability of a drug and stated that a drug shows maximum oral bioavailability if it has the following characteristics (36-38) :

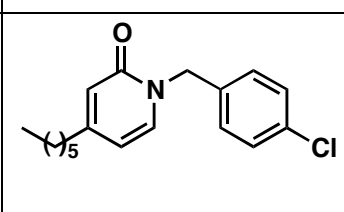
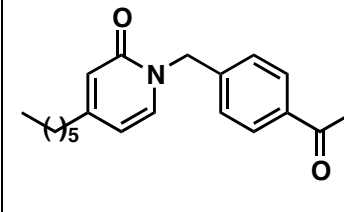
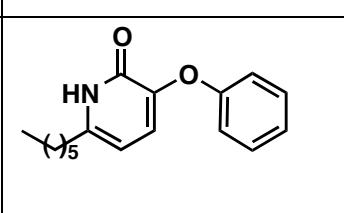
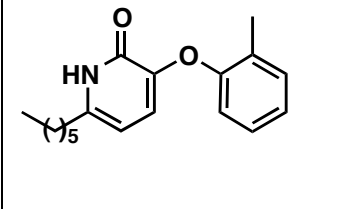
1. Not more than 5 H-bond donors
2. Not more than 10 H-bond acceptors
3. Molecular weight less than 500 g/mol
4. logP (as defined below) less than 5

Lipophilicity of a molecule is defined in terms of logP (37). LogP is the ratio of the solubility of a compound in octanol compared to water. Both diphenyl ethers and the 2-pyridones satisfied the first three Lipinski rules. But for the same substitution pattern, the diphenyl ethers have a greater clogP (calculated logP) as compared to 2-pyridones. In addition, the 2-pyridones are hypothesized to be stable *in vivo* as compared to diphenyl ethers. The –OH group in the A-ring of diphenyl ethers are liable to glucuronidation, a xenobiotic metabolism which decreases the bioavailability of these compounds. This hydroxyl group is essential for inhibition. Hence, in order to reduce the logP and prevent glucuronidation, we synthesized novel 2-pyridone inhibitors. The preliminary inhibition data for inhibition of saFabI is shown in **Table 1**.

Table 1. Inhibition of saFabI by the 2-pyridone inhibitors

Compound	Structure	IC ₅₀ (nM) [E]=50 nM	MIC (μg/mL)	clogP
3		30±10	5	1.04
PT170		>1000	ND	2.95
PT171		150±20	5	5.15
PT172		380±90	5	5.38
PT173		70±10	5	4.58
PT174		250±20	50	4.94
PT175		>1000	50	3.96

Compound	Structure	IC ₅₀ (nM) [E]=50 nM	MIC (μg/mL)	clogP
PT179		190±30	32	4.82
PT420		750±170	32	4.39
PT421		300±60	2	4.97
PT422		220±20	1	4.97
PT423		170±20	16	4.97
PT424		1500±200	ND	4.57
PT425		380±20	~32	3.59

Compound	Structure	IC ₅₀ (nM) [E]=50 nM	MIC (μg/mL)	clogP
PT426		180±20	~32	5.54
PT427		390±40	>128	4.27
PT191		>2000	No inhibition	4.67
PT192		ND	No inhibition	5.17

SAR Analysis

The 2-pyridone compounds synthesized so far are rapid-reversible inhibitors. Moreover, the clogP of these compounds are approximately 5 or lower. Thus, if these inhibitors show good binding affinity and are potent in whole cell assay, then we hypothesize that these compounds will have improved *in vivo* efficacy.

Initially we demonstrated that **PT171** was more potent inhibitor of saFabI with $IC_{50} = 150$ nM as compared to **PT170** with $IC_{50} > 1000$. Hence, we decided to continue our synthesis with hexyl side chain.

B-ring mono-substituents:

The SAR data also shows that as compared to the ortho position, substitution at the para positions would likely result in good inhibition. The residues around the triclosan bound to saFabI are shown in Figure 14. The figure also shows that the B-ring *p*-chloro substituent of triclosan can interact with the backbone of A97. Hence, the inhibition could improve if B-ring *p*-substituents of the 2-pyridone inhibitors can interact with the backbone of A97 similar to triclosan.

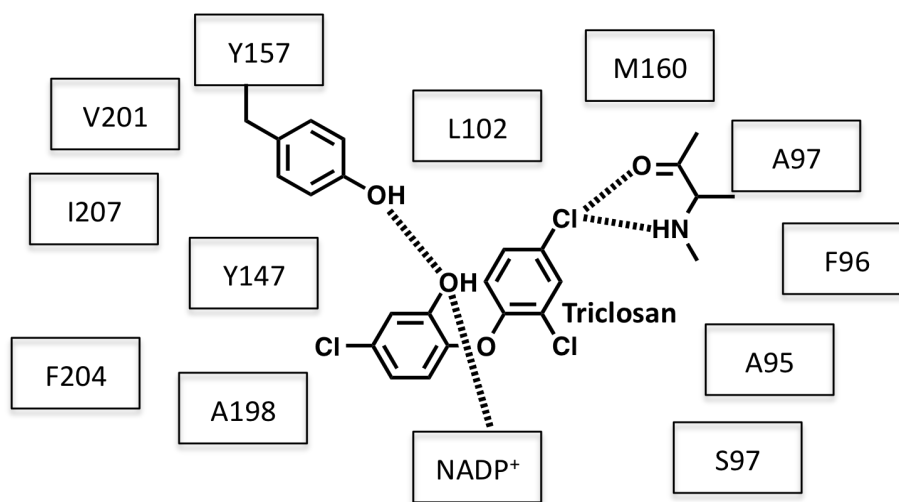


Figure 14. Residues in the active site of saFabI [modified from (33)]

Ortho-position: The data shows that bulky groups at the ortho like –CN (PT420) result in poor inhibition. This could be due to the steric bulk of the cyano group.

PT179 with no B-ring substituent, shows comparable inhibition to analogs with methyl (**PT171**), chloro (**PT172**) and fluoro (**PT423**) substituents. This shows that the *o*- position can tolerate small to moderate sized groups like –H, -Cl, -F, -CH₃. Also, this position can bear electronegative groups like chloro and fluoro groups.

Meta-position: *m*-fluoro substituent in **PT421** has similar inhibition as compared to **PT179**. Thus, this position can tolerate small electronegative groups.

Para-position: The Figure 14 shows that *p*-chloro group of the B-ring can form halogen bonds to the backbone of A97. With this information, we synthesized compound with nitro (**PT424**), amine (**PT425**), chloro (**PT426**) and acetyl (**PT427**) substituents at the *p*- position. As expected, **PT424**, with an electron-withdrawing nitro substituent at this position is disfavored. We expected **PT425**, **PT426** and **PT427** to form halogen or H-bond to the backbone of A97, that would lower the IC₅₀. But the preliminary data shows that these inhibitors show comparable inhibition to **PT179** with no substituent in the B-ring. Further inhibition studies are required in order to understand the interaction of the *p*- substituent with saFabI.

Heterocycles: We also synthesized a compound with heterocyclic fluoro-pyridine (**PT175**) B-ring. Unfortunately this compound showed poor inhibition of saFabI. We need to further analyze such compounds before reaching any conclusion.

Dual substitution: Since compound **3** has *o*-methyl and *m*-NH₂ we wanted to see if we could analyze the effect of this substitution pattern. Hence, we synthesized two compounds, with *o*-methyl *m*-amine (**PT173**), and *o*-methyl *m*-nitro (**PT174**) substituents, respectively. We found that compound **PT173** is the best inhibitor among all the 2-pyridone compounds synthesized with IC₅₀ = 68 nM and MIC = 5 µg/mL. On the other hand **PT174** shows approximately four times lower inhibition as compared to **PT173**. Amine group is H-bond donor and also electron donating while nitro is a bulky electron-withdrawing group. Hence, it is possible that the amine group H-bonds to the FabI, thereby enhancing binding.

A-ring analysis:

The A-ring of **PT191 and PT192** are 2-pyridones that can undergo tautomerism between 2-pyridone and hydroxy-pyridine structures. Moreover, these inhibitors also have bridging oxygen. The rationale behind the synthesis of these compounds was that we wanted to make the A-ring planar and see if the bridging oxygen could enhance binding. To our surprise, we found that this was a very poor inhibitor both *in-vitro* as well as *ex-vivo*. The probable reason for the poor inhibition by these compounds can be explained as follows. As shown in Figure 15, these inhibitors mimic the natural substrate of FabI. On comparison between the two classes of 2-

pyridones, the compounds with bridging methylene are better substrate mimics as compared to the ones with bridging oxygen. As a result, the 2-pyridones with the bridging oxygen have poor IC_{50} .

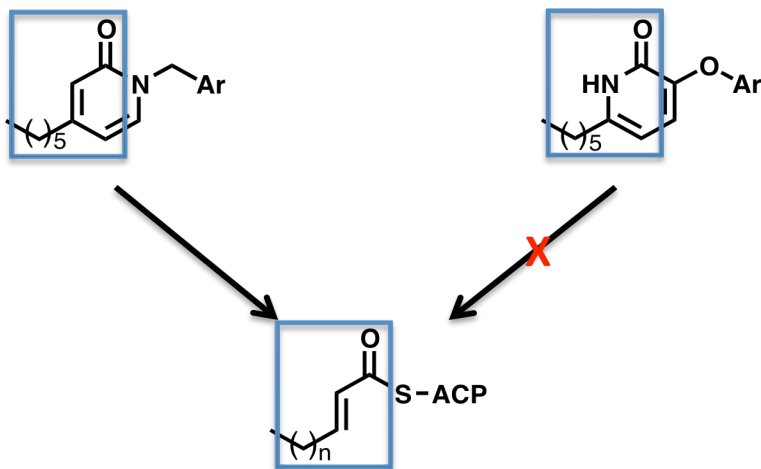


Figure 15. Comparison between the two classes of 2-pyridone inhibitors with the natural substrate of FabI.

The 2-pyridone with bridging methylene (top-left) mimics the natural substrate (bottom-center) better than the 2-pyridone with the bridging oxygen (right).

Conclusion

The 2-pyridone compound library synthesized shows good *in-vivo* and *ex-vivo* activity. The best inhibitor in the series is **PT173** with B-ring similar to **3**. Moreover, these compounds have good MIC and IC_{50} values.

In addition, we were able to increase the hydrophilicity of the inhibitors as compared to their diphenyl ether analog. Different substituents on the B-ring show that it can tolerate a variety of

functional groups for saFabI. Further research is needed to enhance binding and to understand the binding mechanism.

Chapter 3: Inhibition of *Yersinia pestis* enoyl-ACP reductase by the 2-pyridones

Plague is an infectious zoonotic disease caused by the Gram-negative pathogen *Yersinia pestis*. This pathogen was identified by two scientists independently; Alexandre Yersin and Shibasaburo Kitasato (39). History has witnessed devastating plague epidemics. The first epidemic was in 541 A.D. that swept away 50-60% of the population in N. Africa, Europe and Central and southern Asia. Since then there have been many epidemics including the plague of Justinian, Black Death, and Third Pandemic, which has been responsible for millions of death worldwide.

Infected rodents are the carriers for *Y. pestis* that is transmitted to humans via infected body lice, flea and ticks (39, 40). There are three categories of this infection in the order of fatal magnitude: bubonic, septicemic and pneumonic plague. Bubonic and septicemic plague is not transmitted from human to human. In some cases bubonic or septicemic plague develops into secondary pneumonic plague that can spread via respiratory droplets. People who acquire the disease by this route develop pneumonic plague (41). Presently, there is great concern for the use of this pathogen as a biological weapon thereby causing extensive civil disruption. Due to this,

the Center for Disease Control and Prevention (CDC) has classified *Yersinia pestis* as a category A bioterrorism pathogen (42).

For the past 60 years, streptomycin has been used to cure plague. But due to its toxicity, the drug has to be administered cautiously and patients are gradually switched to other antibiotics like tetracycline (39). Presently, due to drug resistant strains, monoclonal antibody therapy is also used for the treatment of plague but is not very efficient (43). US licensed vaccines against this pathogen were discontinued in 1999 as they were effective against bubonic plague but failed to prevent pneumonic plague (41). Thus, as an alternative to vaccine novel and improved drugs are required for the efficient treatment of the disease.

Enoyl ACP reductase FabV

As stated previously, the majority of the enzymes found in the FASII pathway are vital for bacterial viability (44). The last fatty acid elongation step is catalyzed by enoyl-ACP reductase and *Yersinia pestis* is found to have the FabV isoform of this enzyme which was recently discovered in *Vibrio cholera* (45). There are some differences between FabV and FabI. FabV is ~ 60% larger than FabI with sequence similarity limited to ~15%. In addition, the active site sequence of FabV contains Y-(Xaa)₈-K motif, while FabI contains Y-(Xaa)₆-K motif (45, 46).

It has been shown that enoyl-ACP reductases follow different inhibition mechanism and have different binding affinities for inhibitors (47). Thus, in order to target the fatty acid biosynthesis pathway in pathogens containing FabV like *Y. pestis*, novel inhibitors are required.

Project goal

Since the diphenyl ethers are potent inhibitors of FabI from different pathogens we wanted to see if the 2-pyridone compounds that we developed could inhibit ypFabV.

Results and Discussion

While FabI exists as a tetramer in solution, it is quite interesting that ypFabV is a monomer in solution (48). This is consistent with the recent publication showing that FabV from *Vibrio cholerae* (vcFabV) is also a monomer (45).

An interesting difference is observed between FabI and FabV structures. Previously, it has been reported that the substrate-binding loop for binary FabI structure is disordered and becomes ordered in the presence of potent diphenyl ether inhibitors (27). This is due to hydrophobic interactions with the inhibitor that stabilize the substrate-binding loop. On the other hand, the binary FabV structure bound to the cofactor NADH shows that the substrate-binding loop is ordered and does not require further stabilization (48). In this case the substrate-binding loop is stabilized by interactions with the cofactor and a network of H-bonds.

Since the 2-pyridones synthesized are potent inhibitors of saFabI, we wanted to see if these novel inhibitors could inhibit ypFabV. Carla Neckles in our lab, expressed and purified a variant of ypFabV, T276S, and tested the inhibition of 2-pyridones against this mutant. The 2-pyridones are competitive inhibitors of ypFabV with $K_i = 2.1 \pm 0.4 \mu\text{M}$ for **PT172** and $K_i = 1.5 \pm 0.4 \mu\text{M}$ for **PT173**. We were also able to crystallize **PT172** and **PT173** with this mutant (48).

The superimposed image of ternary ypFabV bound to **PT173** and binary FabV bound to NADH is shown in Figure 16. It is interesting to note that the substrate-binding loop moves out by 3 Å when bound to **PT173**.

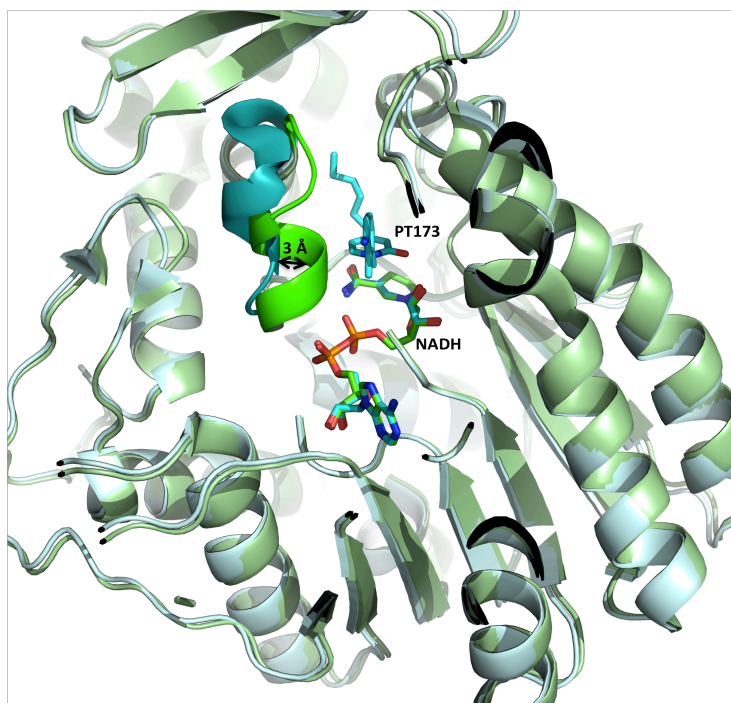


Figure 16. Overlap of apo ypFabV (light green) and ypFabV (light blue) bound to PT173. The substrate binding loops are shown in green and blue respectively (48).

The 2-pyridone inhibitors have interactions with ypFabV similar to the interactions of the diphenyl ether inhibitors of FabI. There is a π - π stacking interaction between the A-ring of 2-pyridone and the nicotinamide ring of NADH. In addition, the carbonyl oxygen of the 2-pyridone

structure forms H-bonds with the active site Y325 and to the nicotinamide ribose. Figure 17 shows additional interaction of the B-ring amine with S141 and S155 via a water molecule. The above results encouraged us to develop SAR for 2-pyridone inhibitors of ypFabV. The inhibition data is shown in **Table 2**.

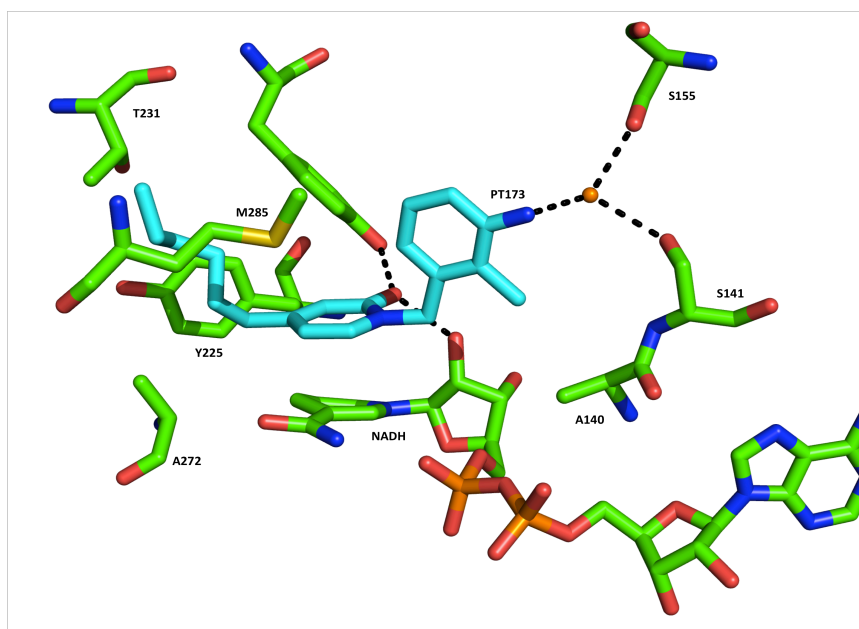
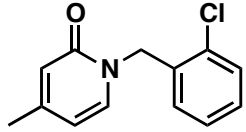
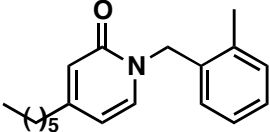
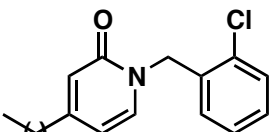
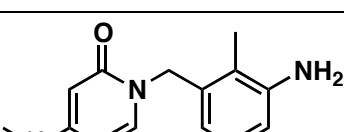
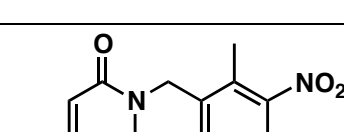
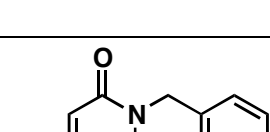
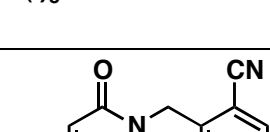
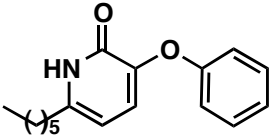
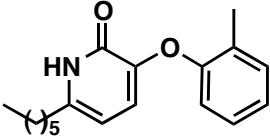


Figure 17. Interactions between PT173 (shown in cyan) with ypFabV residues. H-bonding interactions are shown in black. Conserved water molecule is shown in orange (48).

Table 2. Inhibition of ypFabV by the 2-pyridone inhibitors

Compound	Structure	IC ₅₀ (μM) ^a [E] = 15 nM	clogP
PT170		>100	2.89
PT171		4.0±1	5.28
PT172		2.0±0.3	5.54
PT173		1.0±0.8	3.94
PT 174		3.0±0.5	4.94
PT179		3.0±0.002	4.82
PT420		40.0±5.0	4.39

Compound	Structure	IC ₅₀ (μM) ^a [E] = 15 nM	clogP
PT421		3.0±0.4	4.97
PT422		3.0±0.3	4.97
PT423		2.0±0.4	4.97
PT424		3.0±0.3	4.57
PT425		6.0±1.0	3.59
PT426		2.0±0.3	5.54
PT427		3.0±0.3	4.27

Compound	Structure	IC ₅₀ (μM) ^a [E] = 15 nM	clogP
PT191		16.0±4.0	4.67
PT192		>50	5.17

^a Measured by Carla Neckles

SAR data analysis

Side chain length: On comparison of the chain lengths we found that C-6 alkyl chain on the A ring was better than C-1. There is more than 100-fold difference in inhibition between analogs with methyl (**PT170**) or hexyl (**PT172**) side chains. Because of such a drastic difference in inhibition and the availability of crystal structures of ypFabV bound to **PT172** and **PT173**, we continued our synthesis with hexyl side chain on the A-ring. This side chain mimics the acyl chain of the substrate.

B-ring substituents: To study the effect of substituents on the B-ring, we synthesized **PT179** with no substituent. The inhibition data shows that *o*- position can tolerate different substituents ranging from methyl (**PT171**) to electronegative groups like chloro (**PT172**) and fluoro (**PT423**)

for which the inhibition is within 2-folds. The most surprising result in this category of inhibitors is **PT420** that showed almost a 20-fold lower inhibition compared to **PT172**. This is most likely a steric effect since Cl and CN have nearly identical electro-negativity but cyano has a cylindrical electron potential surface as compared to chloro that has a spherical electron potential surface. This difference in shape of the substituent can lead to difference in IC₅₀ value.

Para position: Next we wanted to evaluate the effect of substituents at the *p*-position. We synthesized and studied the inhibition for fluoro (**PT422**), nitro (**PT424**), amine (**PT425**), chloro (**PT426**) and acetyl (**PT427**) substituents. Our result shows that there is minimal difference in IC₅₀ for these *p*- position substituents. Thus, the *p*-position can tolerate large electronegative substituents such as nitro and H-bonding substituents like amines. The rationale behind the synthesis of **PT425** and **PT427** was that we wanted to see if we could improve the inhibition by replacing the conserved water molecule by the amine group of **PT425** and the carbonyl group of the acetyl side chain in **PT427**. However, the result shows that *p*- substitution has minor effect on the IC₅₀ of the inhibitor.

Dual substituents: Next, we wanted to see if two substituents in the B-ring similar to **3** could improve inhibition. Thus, we synthesized *o*-methyl, *m*-amine (**PT173**) and *o*-methyl, *m*-nitro (**PT174**) substituents. The *m*-amine group of **PT173** shows H-bonding interaction with a conserved water molecule that additionally interacts with S141 and S155. In spite of this favorable interaction, the result shows little and no difference, respectively, in inhibition as

compared to **PT179**. Thus, the *m*- position can tolerate electronegative as well as electron donating substituents even in the presence of an *o*- substituent.

Modified A-ring: In order to study the effect of the bridging oxygen, we synthesized **PT191** and **PT192**. We obtained very surprising and unexpected results. **PT191** with no methyl substituent in B-ring has IC₅₀ of 13 μM that is approximately three-fold higher than **PT179**. On the other hand **PT192** did not inhibit the enzyme even at 50 μM inhibitor concentration. As shown earlier in Figure 15 (Chapter 2), the 2-pyridone inhibitors with bridging methylene are better natural substrate mimics of FabI as compared to the 2-pyridones with bridging oxygen. This is the probable reason that the 2-pyridones with bridging oxygen have high IC₅₀ values.

Conclusion

The above data shows that the 2-pyridones are micro-molar inhibitors of FabV. The crystal structure of ypFabV shows that the substrate-binding loop is ordered both in the binary and ternary forms. Inhibition results show that the substitution pattern on the B-ring does not have a drastic effect on inhibition. In addition, whole cell assays results show that these inhibitors have poor MICs. Thus, there is further scope of improvement of this scaffold.

Chapter 4: Novel diphenyl ethers and mechanistic studies of InhA

Background

Tuberculosis (TB) is an infectious disease caused by different strains of *Mycobacteria*. In humans, it is caused by the pathogen *Mycobacterium tuberculosis* (MTB). MTB usually affects the lungs but it can also affect other parts of the body. This infection spreads through the air from one person to another when the infected person coughs, shouts, sneezes or spits.

MTB resides within the immune system of the host. It has the ability to stay dormant inside the host for a very long time. This elongated dormancy prevents the recognition of the bacteria by the host immune system. The pathogen has developed different mechanisms to survive within the host (49). For example, when MTB is recognized by the macrophage, it is phagocytosed and directed towards fusion with lysosomes. But, MTB is able to diffuse out of the phagolysosome into vacuoles that prevent fusion with secondary lysosomes, thereby preventing lysosomal killing.

Mitchison categorized 4 stages in the life cycle of MTB (50):

1. Having high metabolism and growth rate

2. Semi-dormant in acidic intracellular environment
3. Semi-dormant under non-acidic intracellular environment
4. Dormant

The effective chemotherapy would involve the complete eradication of the rapid growing population followed by the recognition and removal of the semi-dormant and dormant population (51).

The cell wall of MTB is composed of three types of macromolecules that are linked covalently (Figure 18). These are mycolic acid, peptidoglycan and arabinogalactan. Mycolic acids are long chain fatty acids with C-60 to C-90. The peculiar thick hydrophobic cell wall protects the bacterium against antibiotics by preventing their penetration through the cell wall. Since mycolic acids are fatty acids, the fatty acid biosynthesis pathway in MTB was explored as drug target.

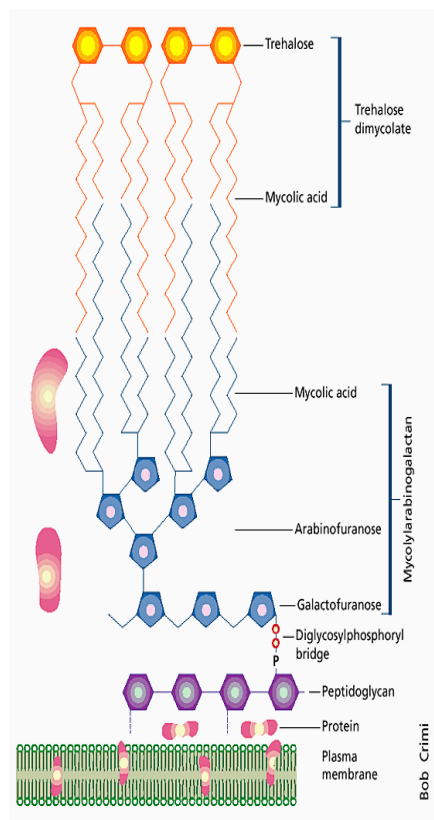


Figure 18. Cell wall of *Mycobacterium tuberculosis* (52)

As stated previously, INH inhibits the FabI in MTB where it is named InhA. Our lab has developed a series of diphenyl ethers that are potent slow onset inhibitors of InhA.

Slow onset inhibition

The majority of the drug discovery efforts are focused on improving the binding affinity of the drug to the target *in vivo*. This concept is based on the determination of thermodynamic parameters such as K_d or K_i or IC_{50} . In addition, whole cell assays like minimal inhibitory concentration (MIC) is used as a measure for determining the potency of a drug. However, *in*

vivo, the concentration of the drug can fluctuate as a function of time and if this falls below the K_d or K_i the drug-target complex can dissociate. On the other hand, in the case of slow-onset inhibition, the drug can remain bound to the target even when the concentration of the drug falls below the K_d or K_i . Thus, it is important to incorporate the lifetime of a drug-target complex as one of the key aspects in drug development. This can be determined by measuring the residence time (t_r) which is the lifetime of the drug-target complex (53).

Slow-onset inhibition can be defined as kinetics of the inhibitor that bind slowly or dissociate slowly from the target. The concept of slow-onset can be explained using Figure 19.

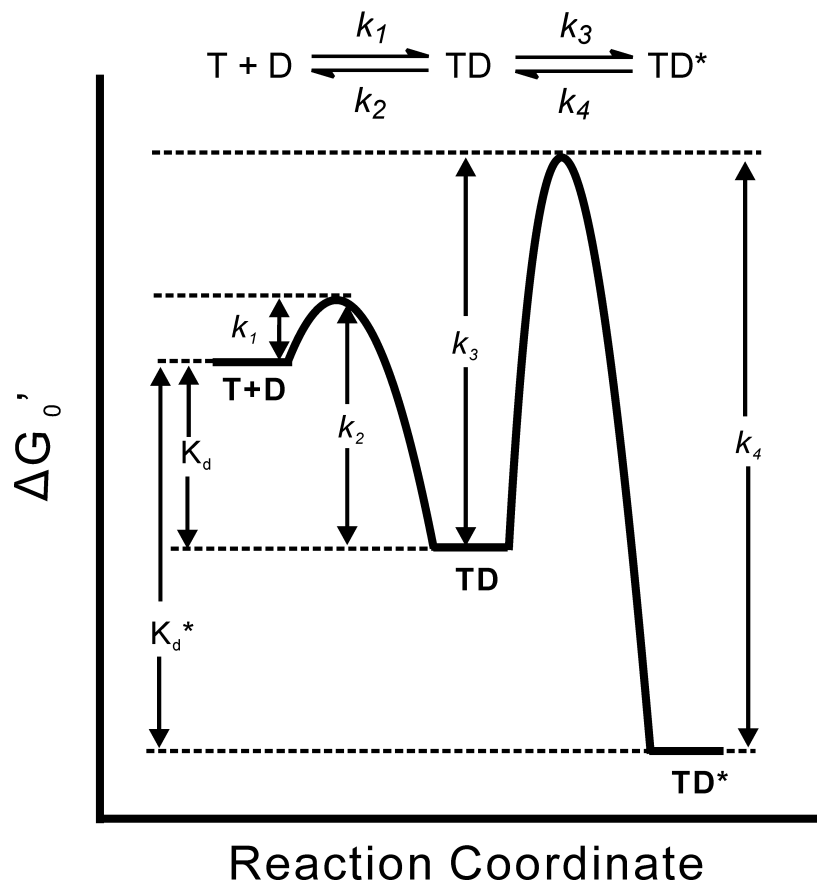


Figure 19. Energy profile for slow-onset inhibition.

The k_1, k_2, k_3, k_4 are the rate constants for each step as shown. K_d and K_d^* are the binding constants for the rapid reversible and slow-onset inhibitor respectively. [figure modified from (53)]

The majority of slow onset inhibitors operate via two-step mechanism. The first step is the rapid formation of the drug-target complex (TD). This is followed by a slow conformational change of this complex leading to the formation of a highly stable drug-target (TD^*) complex (53). Due to this energy barrier, the drug remains bound to the target even if there are fluctuations in drug concentration.

Results and Discussion

Slow-onset inhibitors of InhA

Our lab has synthesized a library of diphenyl ethers that are slow onset inhibitors of InhA. In particular, **PT70**, is a slow-tight binding inhibitor of InhA with $K_i^* = 22$ pM and residence time = 23 min (27).

It was found that **PT70** (Figure 20), which differs from **6PP** only by a methyl group on B ring, is a slow onset inhibitor of InhA. The crystal structure of **PT70** bound to InhA shows that slow onset inhibition is associated with ordering of the substrate-binding loop (Figure 21).

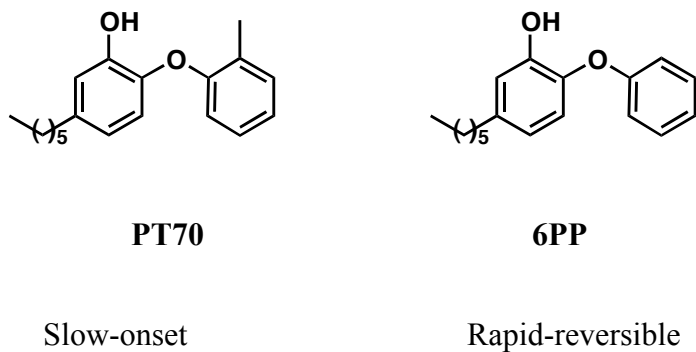


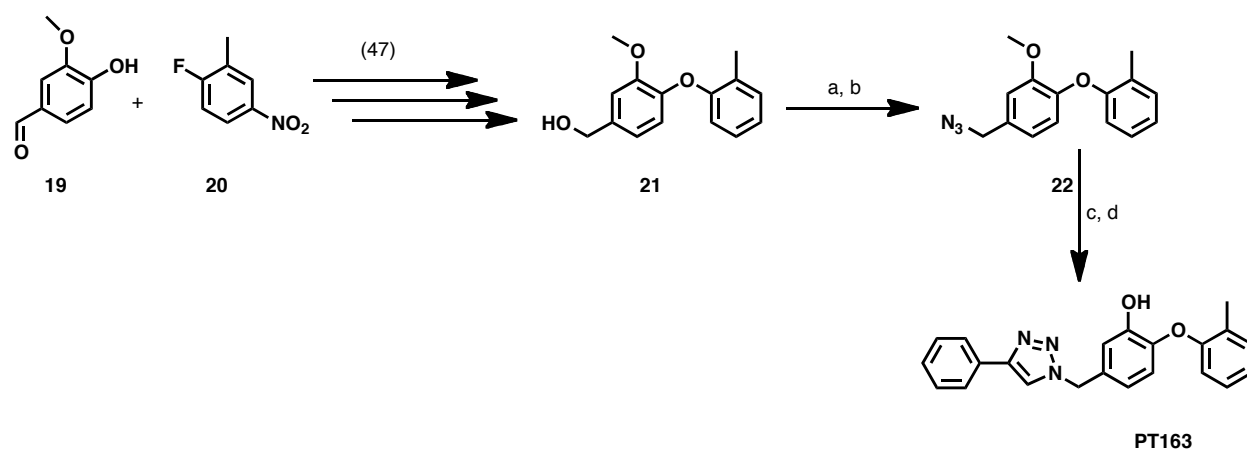
Figure 20. Diphenyl ether inhibitors of InhA.
PT70 is a slow-onset inhibitor while **6PP** is rapid reversible inhibitor



Figure 21. Structure of PT70 bound to InhA.

In cyan is shown the substrate-binding loop that is ordered on binding to **PT70** (shown in beige). The NAD^+ is shown in orange (27).

Although **PT70** is a slow-onset inhibitor, the mechanism of this time dependent inhibition was unknown. Thus, in order to understand the slow-binding mechanism of InhA, we synthesized **PT163**.



Scheme 5. Synthesis of PT163.

Reagent and conditions: a. MsCl , py, DMF, rt, 12h, 70%; b. NaN_3 , DMF, 50°C , 12h, 90%; c. Ethynylbenzene, CuSO_4 , Na-ascorbate, butanol, water, r.t., 5h, 95%; d. BBr_3 , CH_2Cl_2 , -78°C to r.t., 3h, 90%

Synthesis PT163:

Compound **21** was synthesized from commercially available vanillin **19** and 2-fluoro-5-nitrotoulene **20** as described previously (54). Compound **21** was mesylated and treated with sodium azide to form **22**. Finally, compound **22** was subject to click reaction with ethynylbenzene followed by demethylation to give **PT163**.

Discussion

X-ray crystallography, MD simulation and direct measurement of inhibitor dissociation helped us understand the mechanism of time dependent inhibition of InhA. Using MD simulations, two important residues, V203 and Ile215 (shown in Figure 22) were identified that were involved in modulating the transition energy leading to the final inhibitor-enzyme complex.

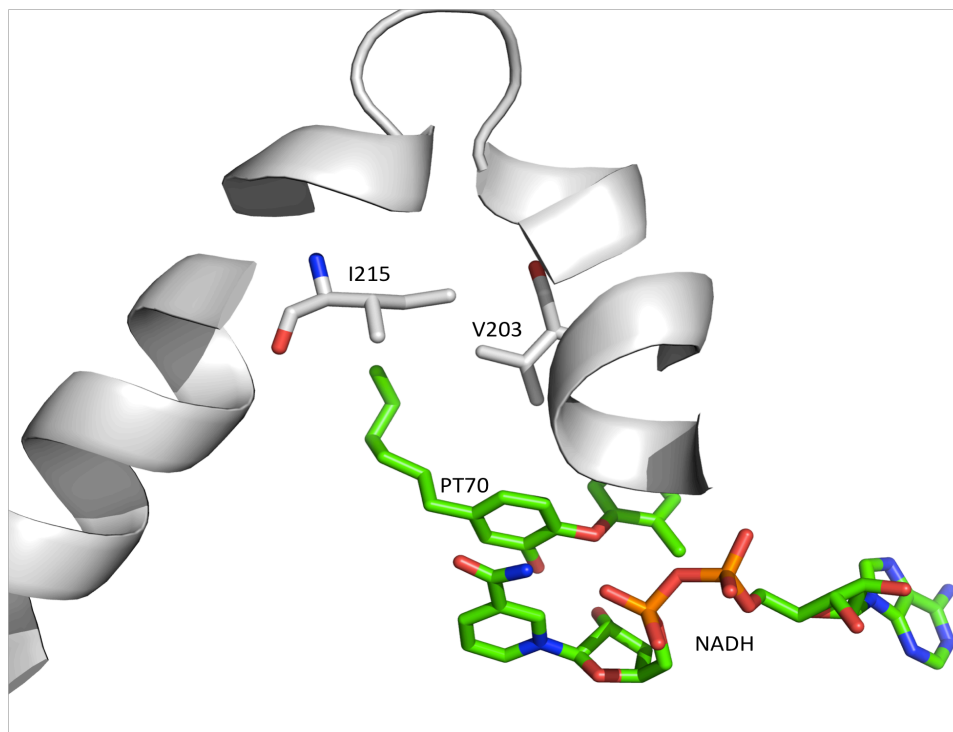


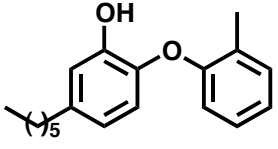
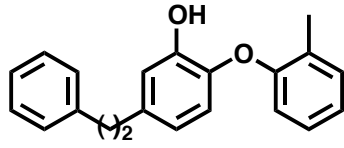
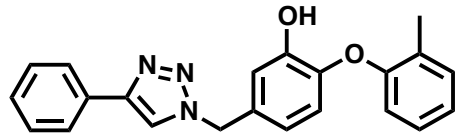
Figure 22. Interactions of PT70 with InhA.

Residues I215 and V203 are shown that are involved in slow-onset binding mechanism (27).

In order to confirm this hypothesis, V203A and I215A mutants were expressed and purified. Kinetic experiments showed that **PT70** lost slow-inhibition with both these mutants. To recover the slow-onset inhibition, **PT162** and **PT163** were synthesized. Both **PT162** and **PT163** have a bulky side chain. In addition to this, **PT163** is even bulkier with two aromatic rings on the side chain.

The result showed that **PT162** is slow-onset for V203A with $t_R = 13.6$ min while it is rapid reversible for I215A. This is so because I215 is located further away from the loop. The interaction between this I215 and the inhibitor was recovered by **PT163**, which is a slow-onset inhibitor of I215A. This result is summarized in **Table 3**.

Table 3. Binding kinetics of diphenyl ethers [Dr. Pan Pan unpublished]

Compound	Structure	Wt InhA	V203A	I215A
PT70		Slow-onset $t_R=24\pm 2$ min	Rapid reversible	Rapid reversible
PT162		Rapid reversible	Slow-onset $t_R=$ 13.6 ± 2.1 min	Rapid reversible
PT163		Slow Onset $t_R=25.3\pm 2.6$ min	ND	Slow-onset $t_R=71.4\pm 4.2$ min

ND: not determined

Conclusion

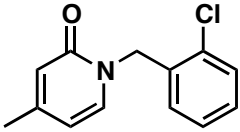
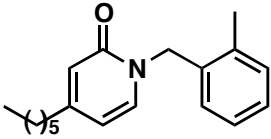
We were able to identify the residues involved in slow-binding mechanism of InhA. MD simulation, X-ray crystallography and kinetic experiments helped in identifying residues, V203 and I215 as the major contributors of slow-onset inhibition of InhA. V203A and Ile215A mutants, and the synthesis of two novel inhibitors **PT162** and **PT163** that helped us validate our hypothesis that V203 and I215 are the major contributors of slow-onset inhibition in InhA.

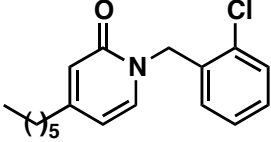
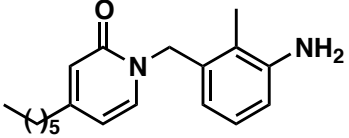
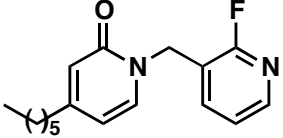
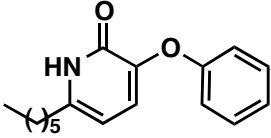
Chapter 5: Future work

Inhibition studies of 2-pyridone inhibitors against other pathogens

Since the 2-pyridone inhibitors are potent inhibitors of saFabI and ypFabV, we were interested to see if these inhibitors could inhibit the FabI enzyme from other pathogens. Thus, we tested some of these inhibitors against FabI enzyme of *Mycobacterium tuberculosis* (InhA), *Francisella tularensis* (ftuFabI) and *Burkholderia pseudomallei* (bpmFabI). Preliminary data is shown in **Table 4**, **Table 5** and **Table 6**, respectively.

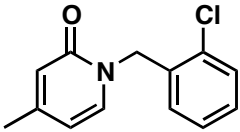
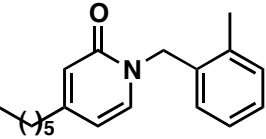
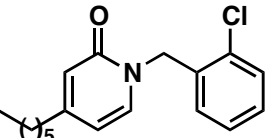
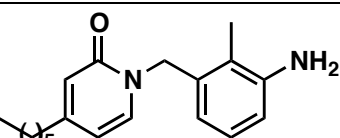
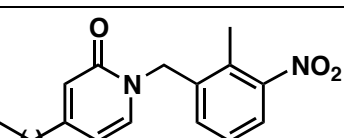
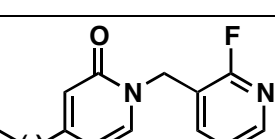
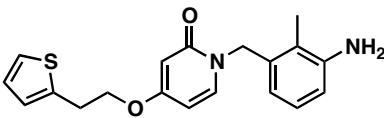
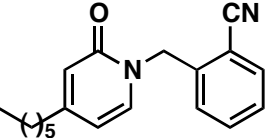
Table 4. Inhibition of InhA by the 2-pyridone inhibitors.

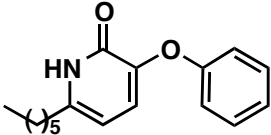
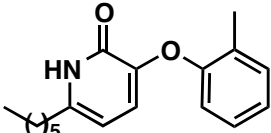
Compound	Structure	IC ₅₀ (nM) [E]=100 nM	MIC ^b (μg/mL)
PT170		>1700	>50
PT171		130±20 [E]= 50nM	25

Compound	Structure	IC ₅₀ (nM) [E]=100 nM	MIC ^b (μg/mL)
PT172		240±40	25
PT173		>3200	50
PT175		>4000	50
PT191		10% inhibition [I]=2uM [E]= 100nM	ND

^b Measured by Jason Cummings at Colorado State University

Table 5. Inhibition of ftuFabI by the 2-pyridone inhibitors

Compound	Structure	IC ₅₀ (nM) ^a [E]=100nM	MIC ^b (μg/mL)
PT170		200±20	50
PT171		80±30	4
PT172		60±10	4
PT173		80±10	4
PT174		80±10	2
PT175		ND	14
3		ND	1
PT420		730±80	10

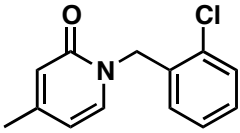
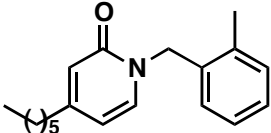
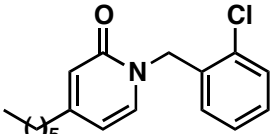
Compound	Structure	IC ₅₀ (nM) ^a [E]=100nM	MIC ^b (μg/mL)
PT191		>10000	ND
PT192		ND	9

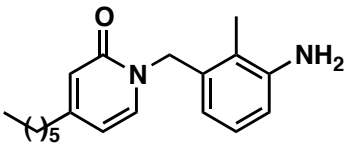
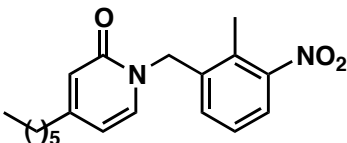
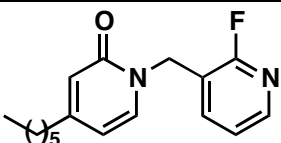
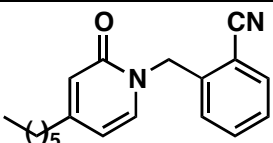
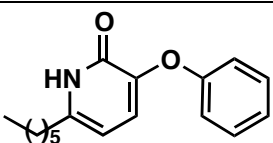
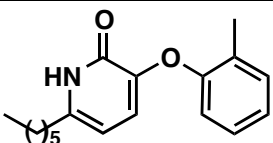
a Measured by Weixuan Yu

b Measured by Jason Cummings at Colorado State University

ND: Not determined

Table 6. Inhibition of bpmFabI by the 2-pyridone inhibitors

Compound	Structure	IC ₅₀ (nM) ^a [E]=30nM	MIC ₉₀ (μg/mL) ^b Bt38
PT170		>1000	ND
PT171		~400	154
PT172		260±9.3	250

Compound	Structure	IC ₅₀ (nM) ^a [E]=30nM	MIC ₉₀ (μg/mL) ^b Bt38
PT173		460±10	36
PT174		ND	250
PT175		>1000	78
PT420		ND	44
PT191		>3000	ND
PT192		ND	8

^a Measured by Hui Wang

^b Measured by Jason Cummings at Colorado State University

The above results show that the 2-pyridone scaffold is promising candidate for inhibition against pathogenic bacteria. Hence, it would be interesting if these inhibitors could be optimized according to the enoyl-ACP reductases from different pathogens.

Future direction

- 1. Detailed mechanistic analysis:** The 2-pyridone inhibitors have different binding mechanism as compared to diphenyl ether. Hence, we need to understand and find out the reason behind this difference in binding mechanism. This would be accomplished by mutagenesis studies on the target enzyme.
- 2. Inhibition studies with other pathogens:** As shown above, 2-pyridones are potent inhibitors of FabI from various pathogens. It would be interesting to understand if we are able to synthesize both broad spectrum as well as pathogen specific inhibitors.
- 3. Slow-onset inhibition:** One of the main focuses of our lab has been the development of slow-onset inhibitors. Although we have many slow onset inhibitors with diphenyl ether scaffold for different enzymes like ftuFabI, InhA and saFabI, so far we know that the 2-pyridone inhibitors are rapid reversible for saFabI (others not tested). Thus, we need to understand and optimize the characteristics of 2-pyridones that would drive slow-onset inhibition for this scaffold.

Chapter 6: Materials and methods

General procedures for compound synthesis:

Reaction A. n-pentyl triphenyl phosphine bromide **5** (10.2 mmol) was taken in dry THF kept under nitrogen at -78 °C. To this n-BuLi (8.9 mmol) was added drop wise. The color of the solution changed to orange. The reaction was stirred for 30 minutes. Then 2-hydroxypyridine-4-carbaldehyde (4.1 mmol) was dissolved in dry DMSO and added drop wise into the r.b. flask. The reaction was kept overnight. After the completion, the reaction the reaction was quenched with NH₄Cl. The THF was evaporated and work up is done using CH₂Cl₂. The product **6** was purified using column chromatography and the product was obtained in 70% ethyl acetate in hexane. After the removal of the solvent, the yield of product was 88% that was a light yellow liquid.

4-((E)-hex-1-enyl)pyridin-2(1H)-one (6):

¹H NMR (500 MHz, CDCl₃): δ 0.89 (t, *J* = 6.5 Hz, 3H), 1.31-1.48 (m, 4H), 2.30-2.35 (m, 2H), 5.82-5.87 (m, 1H), 6.18 (d, *J* = 11.5 Hz, 1H), 6.23 (d, *J* = 6 Hz, 1H), 6.47 (s, 1H), 7.34 (d, *J* = 6 Hz, 1H).

ESI-MS: 178.0 (M+1).

Compound **6** (1 mmol) was dissolved in methanol. To this Pd/C 5% by weight and HCl (1.7 mL, 10%) was added. Then H₂ gas was passed into the r.b. flask. The reaction was completed in 4h. Methanol was evaporated and the work up was done with EtOAc. The yield of the intermediate product **7** was 89% that was a white solid.

4-hexylpyridin-2(1H)-one (7):

¹H NMR (500 MHz, CDCl₃): δ 0.89 (t, *J* = 7 Hz, 3H), 1.27-1.32 (m, 6H), 1.57-1.64 (m, 2H), 2.48 (t, *J* = 8 Hz, 2H), 6.15 (d, *J* = 6 Hz, 1H), 6.39 (s, 1H), 7.27 (d, *J* = 6 Hz, 1H).

¹³C NMR (400 MHz, CDCl₃): δ 14.0, 22.5, 28.7, 29.2, 31.6, 35.7, 108.6, 118.0, 113.6, 158.1, 165.6.

ESI-MS: 180.1 (M+1).

Reaction B. The intermediate **7** (0.3 mmol) and the appropriate benzyl bromide (0.4 mmol) were dissolved in acetonitrile. To this K₂CO₃ (8.23 mmol) was added. The reaction was refluxed for 6h. After the completion, the reaction mixture was filtered and the solvent was evaporated. Work up was done using CH₂Cl₂. The organic layer was dried over MgSO₄ and then purified using column chromatography.

Reaction C. Appropriate benzaldehyde (4 mmol) was dissolved in methanol and cooled to 0 °C. Then NaBH₄ (5.2 mmol) was added in small portions. The color of the solution changes from yellow to colorless. Reaction was completed in 15 mins and then quenched with NH₄Cl. Then,

methanol was evaporated under reduced pressure and the reaction was worked up using ethyl acetate. The product was used without further purification.

The alcohol (3.4 mmol) obtained above was dissolved in dry diethyl ether under argon. To this, PBr₃ (5.1 mmol) was added drop wise. The reaction was completed in 1h. The reaction was quenched by adding water at 0 °C. The reaction was clean and the product is used without further purification.

Reaction D. Compound **9** (1 mmol), CuI (0.1 mmol), picolinic acid (0.2 mmol), ArOH (1.2 mmol) and K₃PO₄ (2 mmol) were dissolved in dry DMSO in r.b. flask under argon. The reaction mixture was heated to 90 °C for 24 h. After the completion, the reaction mixture was cooled to room temperature and work up was done using diethyl ether. The product was purified using column chromatography.

Reaction E. Compound **12** (1 mmol) was added into a solution containing *m*-chloroperbenzoic acid (2.5 mmol) in CHCl₃. The reaction was stirred overnight at room temperature. The reaction mixture was then successively washed with KI (10%), Na₂S₂O₇ (20%), NaOH (10%) and H₂O. The organic layer was collected and the solvent was removed under reduced pressure and the product was purified using column chromatography.

Reaction F. Compound **13** (0.5 mmol) was added into r.b. flask containing acetic anhydride (1.5 mL). The reaction mixture was refluxed for 7 h. The solvent was removed under vacuum. A dark

oily liquid was obtained that is treated with water. This aqueous mixture was heated at 100 °C for 6 h. It was then cooled to room temperature and conc. HCl (1.5 mL) was added to it. This mixture was heated at 90 °C for 24 h. The work up was done using CH₂Cl₂ and it was washed with saturated Na₂CO₃ and brine. The organic layer was then dried over Na₂SO₄. The product was then purified using column chromatography.

Compound Characterization

1-(2-chlorobenzyl)-4-methylpyridin-2(1H)-one (PT170):

2-hydroxy-4-methyl-pyridine (1 mmol) and 2-chloro benzyl bromide (1.2 mmol) were dissolved in acetonitrile and the same procedure was followed, as reaction B. The product obtained was a yellow liquid with 87% yield.

¹H NMR (300 MHz, CDCl₃): δ 2.18 (s, 3H), 5.23 (s, 2H), 6.00-6.03 (dd, *J* = 7.2 Hz, *J* = 1.8 Hz, 1H), 6.43 (br s, 1H), 7.22-7.26 (m, 4H), 7.26-7.39 (m, 1H).

¹³C NMR (400 MHz, CDCl₃): δ 22.1, 51.4, 107.8, 118.2, 126.7, 128.2, 128.7, 129.2, 132.3, 134.5, 136.4, 153.5, 161.3.

ESI-MS: 234.7 (M+1).

1-(2-methylbenzyl)-4-hexylpyridin-2(1H)-one (PT171): Reaction B was used to convert **7** and 2-methylbenzyl bromide to the title product. The product obtained was a brown liquid with 82% yield.

^1H NMR (300 MHz, CDCl_3): δ 0.94 (t, $J = 6.6$ Hz, 3H), δ 1.31-1.40 (m, 6H), δ 1.57-1.65 (m, 2H), δ 2.32 (s, 3H), δ 2.48 (t, $J = 7.5$ Hz, 2H), δ 5.16 (s, 2H), δ 6.03-6.06 (dd, $J = 6.9$ Hz, $J = 1.8$ Hz, 1H), δ 6.49 (d, $J = 1.2$ Hz, 1H), δ 7.00 (d, $J = 6.9$ Hz, 1H), δ 7.09 (d, $J = 6.9$ Hz, 1H), δ 7.21-7.33 (m, 3H).

^{13}C NMR (400 MHz, CDCl_3): δ 13.6, 14.2, 22.1, 28.3, 28.6, 31.1, 34.8, 48.6, 107.5, 118.1, 126.8, 128.7, 129.1, 129.3, 132.8, 133.6, 136.2, 155.3, 162.3.

ESI-MS: 284.1 (M+1).

1-(2-chlorobenzyl)-4-hexylpyridin-2(1H)-one (**PT172**): Reaction B was used to convert **7** and 2-chlorobenzyl bromide to the title product. The product obtained was a light yellow solid with 88% yield.

^1H NMR (500 MHz, CDCl_3): δ 0.92 (t, $J = 10$ Hz, 3H), 1.32-1.38 (m, 6H), 2.48 (t, $J = 8$ Hz, 2H), 5.26 (s, 2H), 6.06 (d, $J = 7$ Hz, 1H), 6.45 (s, 1H), 7.20-7.29 (m, 4H), 7.42 (m, 2H)

^{13}C NMR (400 MHz, CDCl_3): δ 13.9, 22.8, 27.1, 29.1, 32.5, 35.4, 49.5, 108.2, 117.8, 127.8, 128.9, 129.5, 130.1, 133.4, 134.2, 135.5, 155.6, 161.5

ESI-MS: 304.8 (M+1).

1-(2-methyl-3-nitrobenzyl)-4-hexylpyridin-2(1H)-one (**PT174**): Reaction B was used to convert **7** and 3-nitro-2-methyl-benzylbromide to the title product. The product obtained was a brown liquid with 89% yield.

^1H NMR (300 MHz, CDCl_3): δ 0.87 (t, $J = 6.9$ Hz, 3H), 1.23-1.32 (m, 6H), 1.51-1.53 (m, 2H), 2.41 (s, 3H), 2.45 (t, $J = 7.2$ Hz, 2H), 5.17 (s, 2H), 6.06 (dd, $J = 1.8, 7.2$ Hz, 1H), 7.02 (d, $J = 7$ Hz, 1H), 7.17 (d, $J = 7.5$ Hz, 1H), 7.27 (m, 1H), 7.69 (dd, $J = 1, 8$ Hz, 1H)

^{13}C NMR (500 MHz, CDCl_3): δ 13.9, 14.4, 22.3, 28.6, 28.9, 31.4, 35.1, 49.2, 108.4, 118.4, 123.3, 126.6, 131.4, 135.7, 137.2, 151.3, 155.9, 162.4.

ESI-MS: 329.1 (M+1).

1-(3-amino-2-methylbenzyl)-4-hexylpyridin-2(1H)-one (**PT173**): Zn (1.3 mmol), NH_4Cl (1.9 mmol), and **PT174** (0.13 mmol) were dissolved in 1:5 water and methanol. The reaction was heated to 65 °C for half hour. The solvent was removed under reduced pressure. The product was purified using column chromatography. The product obtained was a light yellow solid with 90% yield.

^1H NMR (300 MHz, CDCl_3): δ 0.89 (t, $J = 8$ Hz, 3H), 1.24-1.28 (m, 8H), 2.01 (s, 3H), 2.40 (t, $J = 7.8$ Hz, 2H), 3.7 (br s, 2H), 5.10 (s, 2H), 5.93-5.95 (dd, $J = 7.2$ Hz, 8.7 Hz, 1H), 6.41 (br s, 1H), 6.59 (d, $J = 3$ Hz, 1H), 6.71 (d, $J = 8$ Hz, 2H), 6.94 (d, $J = 6$ Hz, 1H), 7.03 (t, $J = 6$ Hz, 1H).

^{13}C NMR (500 MHz, CDCl_3): δ 13.9, 22.5, 28.7, 29.0, 31.5, 35.2, 49.1, 108.0, 118.6, 127.2, 129.1, 129.5, 130.0, 133.4, 134.0, 136.4, 155.7, 162.8.

ESI-MS: 299.1 (M+1).

1-benzyl-4-hexylpyridin-2(1H)-one (**PT179**): Reaction B was used to convert **7** and benzylbromide to the title product. The product obtained was a yellow liquid with 90% yield.

¹H NMR (500 MHz, CDCl₃): δ 0.84 (t, *J* = 7 Hz, 3H), 1.26-1.32 (m, 6H), 1.5-1.56 (m, 2H), 2.38 (t, *J* = 5 Hz, 2H), 5.08 (s, 2H), 5.97 (d, *J* = 7 Hz), 6.39 (s, 1H), 7.11 (d, *J* = 7 Hz, 1H), 7.24-7.32 (m, 5H)

¹³C NMR (400 MHz, CDCl₃): δ 13.9, 22.5, 22.7, 29.0, 31.5, 35.2, 51.4, 108.0, 118.7, 127.8, 128.1, 128.8, 136.1, 136.6, 155.5, 162.8.

ESI-MS: 270.2 (M+1).

2-((4-hexyl-2-oxopyridin-1(2H)-yl)methyl)benzotrile (**PT420**): Reaction B was used to convert **7** and 2-cyano-benzylbromide to the title product. The product obtained was a dark yellow liquid with 92% yield.

¹H NMR (500 MHz, CDCl₃): δ 0.88 (t, *J* = 7 Hz, 3H), 1.25-1.34 (m, 6H), 1.54-1.63 (m, 2H), 2.43 (t, *J* = 8 Hz, 2H), 5.31 (s, 2H), 6.07 (d, *J* = 7.5 Hz, 2H), 6.42 (s, 1H), 7.34 (d, *J* = 7.5 Hz, 1H), 7.38-7.41 (m, 2H), 7.53-7.55 (m, 1H), 7.66 (d, *J* = 8 Hz, 1H)

¹³C NMR (400 MHz, CDCl₃): δ 13.9, 22.4, 28.7, 28.9, 31.5, 35.2, 49.9, 108.4, 111.6, 117.6, 118.7, 128.3, 129.7, 132.7, 133.3, 136.6, 140.1, 156.2, 162.6.

ESI-MS: 295.3 (M+1)

1-(3-fluorobenzyl)-4-hexylpyridin-2(1H)-one (PT421): Reaction C was used to convert 3-fluorobenzaldehyde to 3-fluorobenzylbromide. This crude 3-fluorobenzylbromide was then reacted with **7** according to Reaction B to obtain the title product. The product obtained was a yellow liquid with 87% yield.

¹H NMR (500 MHz, CDCl₃): δ 0.86-0.89 (m, 3H), 1.26-1.35 (m, 8H), 2.39 (t, *J* = 8 Hz, 3H), 5.08 (s, 2H), 6.02 (d, *J* = 7 Hz, 1H), 6.41 (s, 1H), 7.04 (d, *J* = 7 Hz, 1H), 6.94-6.98(m, 1H), 7.15-7.29 (m, 3H).

¹³C NMR (400 MHz, CDCl₃): δ 13.9, 22.4, 28.7, 28.9, 31.4, 35.1, 50.95, 108.1, 114.6, 114.8 (dd), 118.6, 123.4, 130.3(d), 136.1, 139.0 (d), 155.7, 161.9, 162.6, 163.9.

ESI-MS: 288.2 (M+1).

1-(4-fluorobenzyl)-4-hexylpyridin-2(1H)-one (PT422): Reaction C was used to convert 4-fluorobenzaldehyde to 4-fluorobenzylbromide. This crude 4-fluorobenzylbromide was then reacted with **7** according to Reaction B to obtain the title product. The product obtained was a light yellow liquid with 85% yield.

¹H NMR (500 MHz, CDCl₃): δ 0.89 (t, *J* = 7Hz, 3H), δ 1.30 (m, 6H), δ 1.57 (m, 2H), δ 2.42 (t, 2H), 5.08 (s, 2H), 6.03 (dd, *J* = 1.5, 7 Hz), 6.42 (s, 1H), 7.023 (m, 2H), δ 7.16 (m, 1H), δ 7.30 (m, 1H).

¹³C NMR (400 MHz, CDCl₃): δ 13.9, 22.5, 28.7, 29.0, 31.5, 35.2, 50.9, 108.2, 115.5, 115.8, 118.8, 129.9 (d), 132.4 (d), 136.0, 155.7, 161.4, 162.7, 163.4.

ESI-MS: 288.2 (M+1).

1-(2-fluorobenzyl)-4-hexylpyridin-2(1H)-one (**PT423**): Reaction C was used to convert 2-fluorobenzaldehyde to 2-fluorobenzylbromide. This crude 2-fluorobenzylbromide was then reacted with **7** according to Reaction B to obtain the title product. The product obtained was a yellow liquid with 88% yield.

¹H NMR (500 MHz, CDCl₃): δ 0.87 (t, *J* = 5.5 Hz, 3H), 1.28 (m, 6H), 1.56-1.59 (m, 2H), 2.40 (t, *J* = 8 Hz, 2H), 5.13 (s, 2H), 6.38 (s, 1H), 7.07 (m, 2H), 7.23 (m, 1H), 7.40 (m, 1H).

¹³C NMR (400 MHz, CDCl₃): δ 14.0, 22.5, 28.8, 29.1, 31.6, 35.3, 45.6(d), 108.1, 115.3, 115.5, 118.7, 124.5 (d), 129.8 (d), 131.3 (d), 136.5 (d), 160.5, 161.8, 162.9.

ESI-MS: 288.1 (M+1).

1-(4-nitrobenzyl)-4-hexylpyridin-2(1H)-one (**PT424**): Reaction C was used to convert 4-nitrobenzaldehyde to 4-nitrobenzylbromide. This crude 4-nitrobenzylbromide was then reacted with **7** according to Reaction B to obtain the title product. The product obtained was a yellow liquid with 80% yield.

¹H NMR (500 MHz, CDCl₃): δ 0.90 (t, *J* = 7 Hz, 3H), 1.27-1.35 (m, 6H), 1.59-1.60 (m, 2H), 2.47 (t, *J* = 7.5 Hz, 2H), 5.22 (s, 2H), 6.13 (dd, *J* = 1.5, 7 Hz, 1H), 6.52 (s, 1H), 7.21 (d, *J* = 7 Hz, 1H), 7.45 (d, *J* = 8.5 Hz, 2H), 8.21 (m, 2H).

^{13}C NMR (400 MHz, CDCl_3): δ 13.9, 14.4, 28.5, 29.1, 31.5, 35.1, 50.2, 108.1, 115.5, 118.6, 131.4, 135.3, 138.2, 152.0, 155.3, 171.0.

ESI-MS: 316.1 (M+1).

1-(4-aminobenzyl)-4-hexylpyridin-2(1H)-one (**PT425**): Zn (1.3 mmol), NH_4Cl (1.9 mmol), and **PT424** (0.13 mmol) were dissolved in 1:5 water and methanol. The reaction was heated to 65 °C for half hour. The solvent was removed under reduced pressure. The product was purified using column chromatography. The product obtained was a yellow liquid with 89% yield.

^1H NMR (300 MHz, CDCl_3): δ 0.93 (t, $J = 6.9$ Hz, 3H), 1.31-1.33 (m, 6H), 1.56-1.62 (m, 2H), 2.45 (t, $J = 7.5$ Hz, 2H), 3.62 (br s), 5.03 (s, 2H), 6.03 (dd, $J = 1.8, 7.2$ Hz, 1H), 6.45 (s, 2H), 6.67-6.71 (m, 2H), 7.15-7.21 (m, 2H)

^{13}C NMR (300 MHz, CDCl_3): δ 14.0, 22.5, 28.7, 29.0, 31.5, 35.1, 50.9, 107.9, 115.2, 118.4, 126.1, 129.7, 135.9, 146.1, 155.3, 171.2

ESI-MS: 285.2 (M+1)

1-(4-chlorobenzyl)-4-hexylpyridin-2(1H)-one (**PT426**): Reaction C was used to convert 4-chlorobenzaldehyde to 4-chlorobenzylbromide. This crude 4-chlorobenzylbromide was then reacted with **7** according to Reaction B to obtain the title product. The product obtained was a yellow liquid with 92% yield.

¹H NMR (400 MHz, CDCl₃): δ 0.89 (t, *J* = 7 Hz, 3H), 1.28-1.34 (m, 6H), 1.54-1.57 (m, 2H), 2.42 (t, *J* = 7.5 Hz, 2H), 5.07 (s, 2H), 6.02 (d, *J* = 6.5 Hz, 1H), 6.42 (s, 1H), 7.15 (m, 2H), 7.23-7.32 (m, 4H).

¹³C NMR (400 MHz, CDCl₃): δ 14.0, 22.5, 28.7, 29.0, 31.5, 35.2, 50.9, 108.2, 118.8, 128.9, 129.4, 133.8, 135.1, 135.9, 155.7, 162.6.

ESI-MS: 304.3 (M+1).

1-(4-acetylbenzyl)-4-hexylpyridin-2(1H)-one (**PT427**): Reaction C was used to convert 4-acetylbenzaldehyde to 4-acetylbenzylbromide. This crude 4-acetylbenzylbromide was then reacted with **7** according to Reaction B to obtain the title product. The product obtained was a yellow solid with 82% yield.

¹H NMR (400 MHz, CDCl₃): δ 0.88 (t, *J* = 6.8 Hz, 3H), 1.26-1.35 (m, 6H), 1.55-1.59 (m, 2H), 2.44 (t, *J* = 7.7 Hz, 2H), 2.58 (s, 3H), 5.17 (s, 2H), 6.05-6.07 (dd, *J* = 1.32, 7 Hz, 1H), 6.46 (s, 1H), 7.17 (d, *J* = 7Hz, 1H), 7.37 (d, *J* = 8.1 Hz, 2H), 7.92 (d, *J* = 8.1 Hz, 2H).

¹³C NMR (400 MHz, CDCl₃): δ 13.9, 22.5, 26.6, 28.7, 29.0, 29.6, 31.5, 35.3, 51.4, 108.5, 118.8, 127.9, 128.8, 136.1, 136.6, 141.8, 156.0, 162.6, 197.5.

ESI-MS: 312.4 (M+1).

6-hexyl-3-phenoxy pyridin-2(1H)-one (**PT191**): Reaction F was used to convert compound **13a** to the title product. The product obtained was a yellow liquid with 30% yield.

^1H NMR (300 MHz, CDCl_3): δ 0.87 (t, $J = 7$ Hz, 3H), 1.23-1.29 (m, 6H), 1.55-1.60 (m, 2H), 2.47 (t, $J = 7.5$ Hz, 2H), 5.92 (d, $J = 7.5$ Hz, 1H), 6.96 (d, $J = 7.5$ Hz, 1H), 7.01-7.02 (m, 2H), 7.03-7.05 (m, 2H), 7.31-7.32 (m, 2H).

^{13}C NMR (500 MHz, CDCl_3): δ 13.9, 22.5, 28.4, 28.6, 31.4, 32.6, 103.7, 117.7, 122.9, 127.3, 129.5, 143.8, 144.9, 157.0, 160.4.

ESI-MS: 272.1 (M+1).

3-(o-tolyloxy)-6-hexylpyridin-2(1H)-one (**PT192**): Reaction F was used to convert compound **13b** to the title product. The product obtained was a yellow liquid with 25% yield.

^1H NMR (500 MHz, CDCl_3): δ 0.88 (t, $J = 7.5$ Hz, 3H), 1.28-1.317 (m, 6H), 1.59-1.64 (m, 2H), 2.3 (s, 3H), 2.52 (t, $J = 7.5$ Hz, 2H), 5.89 (d, $J = 7.5$ Hz, 1H), 6.73 (d, $J = 7.5$ Hz, 1H), 6.89 (d, $J = 7.5$ Hz, 1H), 7.05 (t, $J = 7.5$ Hz, 1H), 7.15 (t, $J = 7.5$ Hz, 1H), 7.24 (d, $J = 7.5$ Hz, 1H).

^{13}C NMR (500 MHz, CDCl_3): δ 13.9, 16.1, 22.5, 28.4, 28.5, 31.5, 32.6, 103.6, 118.5, 123.8, 124.0, 126.9, 129.2, 131.3, 143.4, 144.9, 154.4, 160.0.

ESI-MS: 286.0 (M+1).

6-hexyl-3-phenoxy pyridin-2(1H)-one (**12a**): n-pentyl triphenyl phosphine bromide **5** (10.2 mmol) was taken in dry THF kept under nitrogen at -78 °C. To this n-BuLi (8.9 mmol) was added drop wise. The color of the solution changes to orange. The reaction was stirred for 30 minutes. Then 5-Bromo-pyridine-2-carbaldehyde (4.1 mmol) was dissolved in dry DMSO and added drop wise

into the r.b. flask. The reaction was kept overnight. After the completion, the reaction the reaction is quenched with NH₄Cl. The THF was evaporated and work up is done using CH₂Cl₂. The product **11** was purified and coupled with phenol using Reaction D. This was then catalytically hydrogenated in the presence of Pd/C 5% by weight and HCl (0.5 mL) to obtain compound **12a**. The product obtained was a dark yellow liquid with 85% yield.

¹H NMR (500 MHz, CDCl₃): δ 0.89 (t, *J* = 7 Hz, 3H), 1.27-1.39 (m, 6H), 1.70-1.76 (m, 2H), 2.78 (t, *J* = 8 Hz, 2H), 7.01 (d, *J* = 8 Hz, 1H), 7.12 (d, *J* = 8.5 Hz, 1H), 7.22-7.24 (m, 2H), 7.35 (m, 2H), 8.36 (d, *J* = 2.5 Hz, 1H).

¹³C NMR (500 MHz, CDCl₃): δ 14.0, 22.6, 29.0, 29.9, 31.7, 37.6, 118.4, 122.9, 123.5, 126.4, 129.8, 140.8, 151.5, 157.0, 157.4.

ESI-MS: 256.2 (M+1).

3-(o-tolyloxy)-6-hexylpyridin-2(1H)-one (12b): The title product was obtained by performing similar reactions as for **12a**. The coupling was done using *o*-cresol. The product obtained was a yellow liquid with 87% yield.

¹H NMR (500 MHz, CDCl₃): δ 1.07 (t, *J* = 7 Hz, 3H), 1.45-1.55 (m, 6H), 1.85-1.93 (m, 2H), 2.5 (s, 3H), 2.95 (t, *J* = 8.5 Hz, 2H), 7.05 (d, *J* = 7 Hz, 1H), 7.24-7.27 (m, 3H), 7.29-7.37 (m, 2H), 7.45 (d, *J* = 7 Hz, 1H), 7.98 (d, *J* = 2.5 Hz, 1H).

¹³C NMR (500 MHz, CDCl₃): δ 14.0, 16.1, 22.5, 28.9, 29.9, 31.6, 37.4, 118.9, 122.8, 124.2, 124.6, 127.2, 129.5, 131.5, 131.5, 131.5, 139.5, 151.9, 154.0, 156.4.

ESI-MS: 270.0 (M+1).

*6-hexyl-3-phenoxy*pyridin-*N*-oxide-2(1*H*)-one (**13a**): Reaction E was used to oxidized compound **12a** into the title product. The product obtained was a dark yellow liquid with 50% yield.

¹H NMR (300 MHz, CDCl₃): δ 0.88 (t, *J* = 7.5 Hz, 3H), 1.24-1.43 (m, 6H), 1.64-1.74 (m, 2H), 2.86 (t, *J* = 8.1 Hz, 2H), 6.92 (d, *J* = 7 Hz, 1H), 7.15-7.20 (m, 3H), 7.34-7.41 (m, 2H), 7.45 (d, *J* = 7 Hz, 1H), 8.02 (d, *J* = 2.1 Hz, 1H).

ESI-MS: 272.4 (M+1).

*3-(o-tolyloxy)-6-hexyl*pyridin-*N*-oxide-2(1*H*)-one (**13b**): Reaction E was used to oxidized compound **12b** into the title product. The product obtained was a dark yellow liquid with 46% yield.

¹H NMR (500 MHz, CDCl₃): δ 0.94 (t, *J* = 7 Hz, 3H), 1.36-1.45 (m, 6H), 1.71-1.77 (m, 2H), 2.25 (s, 3H), 2.91 (t, *J* = 7.5 Hz, 2H), 6.86-6.88 (m, 1H), 7.01 (d, *J* = 8 Hz, 1H), 7.15-7.25 (m, 2H), 7.25-7.28 (m, 1H), 7.31 (d, *J* = 8Hz, 1H), 7.98 (d, *J*=2 Hz, 1H).

ESI-MS: 286.1 (M+1).

*1-(2-methyl-3-nitrobenzyl)-4-(benzyloxy)*pyridin-2(1*H*)-one (**17**): Reaction B was used to convert the starting material 4-(Benzyloxy)pyridin-2(1*H*)-one and 3-nitro-2-methyl-benzylbromide to the title product. The product obtained was a yellow liquid with 84% yield.

^1H NMR (500 MHz, CDCl_3): δ 2.26 (s, 3H), 4.87 (s, 2H), 4.99 (s, 2H), 5.87-5.91 (m, 2H), 6.89 (d, $J = 7.5$ Hz, 1H), 7.03 (d, $J = 7.5$ Hz, 1H), 7.14-7.17 (m, 3H), 7.22-7.25 (m, 3H), 7.56 (d, $J = 8$ Hz).

^{13}C NMR (500 MHz, CDCl_3): δ 14.4, 48.9, 70.2, 98.2, 101.9, 123.4, 126.7, 127.7, 128.5, 128.6, 130.3, 131.2, 134.8, 136.6, 137.2, 151.2, 163.7, 167.1.

ESI-MS: 351.0 (M+1).

1-(3-amino-2-methylbenzyl)-4-hydroxypyridin-2(1H)-one (**18**): Title product was obtained by catalytic hydrogenation of compound **17** similar to that shown in Reaction A.

ESI-MS: 231.1 (M+1).

1-benzyl-4-(pentyloxy)pyridin-2(1H)-one (**3**): Compound **18** (1 mmol) and 2-(2-Bromoethyl) thiophene (1.2 mmol), Cs_2CO_3 (1.2 mmol) and NaI (0.1 mmol) were dissolved in DMF at room temperature. The reaction was stirred for 12 h. After the completion of the reaction, work up was done using diethyl ether. The product was purified and the yield of product obtained was 80% [Predicted NMR and ^{13}C NMR shifts are given in (55)].

^1H NMR (500 MHz, CDCl_3): δ 2.00 (s, 3H), 3.28 (t, $J = 6.5$ Hz, 3H), 3.61-3.79 (br s, 2H), 4.13 (t, $J = 6.5$ Hz, 3H), 5.04 (s, 2H), 5.84 (dd, $J = 3$ Hz, 8 Hz, 1H), 5.93 (d, $J = 2.5$ Hz, 1H), 6.56 (d, $J = 7$ Hz, 1H), 6.68 (d, $J = 8$ Hz, 1H), 6.87-6.99 (m, 2H), 7.16 (dd, $J = 1$ Hz, 5.5 Hz, 1H).

^{13}C NMR (500 MHz, CDCl_3): δ 12.3, 29.6, 49.1, 68.3, 97.5, 100.9, 115.5, 120.3, 120.9, 124.1, 125.6, 126.7, 126.8, 134.6, 136.2, 139.5, 145.4, 163.1, 166.7.

ESI-MS: 341.1 (M+1).

Measurement of IC_{50}

The experiments were carried out in Cary 100 Bio (Varian) spectrophotometer at 25°C . Kinetic assay was performed using DD-CoA and saFabI. Buffer used is 50 mM potassium phosphate, 150 mM sodium chloride and 350 mM potassium glutamate at pH 7.5. The assay contains $300\mu\text{M}$ NADPH, $20\mu\text{M}$ DD CoA and 50 nM enzyme. The IC_{50} was determined by varying the concentration of inhibitor from 0 to $2\mu\text{M}$. The inhibitor solution was prepared in DMSO. The reaction is initiated by the addition of 50 nM enzyme. IC_{50} was determined using the equation (1):

$$y = 100\% / [1 + (I/\text{IC}_{50})] \quad (1)$$

y = percent activity, I= inhibitor concentration

Data fitting was performed using GraFit 4.0.

MIC for *S. aureus* were determined by Yang Lu in Tonge Lab. MIC for *M. tuberculosis*, *Y. Pestis*, *F. tularensis* and *B. pseudomallei* were performed by our collaborators at Colorado State University.

Synthesis of trans-2-Dodecenoyl-CoA (DDCoA).

DDCoA was synthesized from trans-2-decenoic acid using the mixed anhydride method as described previously (56).

Expression and Purification of enzymes

saFabI was expressed and purified as described previously (57).

ypFabV was expressed and purified by Carla Neckles (Tonge Lab).

ftuFabI, bpmFabI and inhA were expressed and purified Dr. Nina Liu.

Enzymatic studies, X-ray crystallography and MD simulations were conducted by Dr. Pan Pan, Huei Jiun Li and Cheng-Tsung Lai, respectively.

PT162 was synthesized by Dr Gopal B. Reddy.

References

1. Landsberg, H. (1949) Prelude to the discovery of Penicillin, *Isis* 40, 225-227.
2. Bosch, F., and Rosich, L. (2008) The contributions of Paul Ehrlich to pharmacology: a tribute on the occasion of the centenary of his Nobel Prize, *Pharmacology* 82, 171-179.
3. Fleming, A. (1941) Penicillin, *Br. Med. J.* 2, 386-386.
4. Wright, G. D. (2007) The antibiotic resistome: the nexus of chemical and genetic diversity, *Nat Rev Microbiol* 5, 175-186.
5. Lu, H., and Tonge, P. J. (2008) Inhibitors of FabI, an enzyme drug target in the bacterial fatty acid biosynthesis pathway, *Acc Chem Res* 41, 11-20.
6. White, S. W., Zheng, J., Zhang, Y. M., and Rock. (2005) The structural biology of type II fatty acid biosynthesis, *Annu Rev Biochem* 74, 791-831.
7. Levy, S. B., and Marshall, B. (2004) Antibacterial resistance worldwide: causes, challenges and responses, *Nat Med* 10, S122-129.
8. McDevitt, D., and Rosenberg, M. (2001) Exploiting genomics to discover new antibiotics, *Trends Microbiol* 9, 611-617.
9. Campbell, J. W., and Cronan, J. E., Jr. (2001) Bacterial fatty acid biosynthesis: targets for antibacterial drug discovery, *Annu Rev Microbiol* 55, 305-332.
10. Payne, D. J., Warren, P. V., Holmes, D. J., Ji, Y., and Lonsdale, J. T. (2001) Bacterial fatty-acid biosynthesis: a genomics-driven target for antibacterial drug discovery, *Drug Discov Today* 6, 537-544.

11. Egan, A. F., and Russell, R. R. (1973) Conditional mutations affecting the cell envelope of *Escherichia coli* K-12, *Genet Res* 21, 139-152.
12. Turnowsky, F., Fuchs, K., Jeschek, C., and Hogenauer, G. (1989) envM genes of *Salmonella typhimurium* and *Escherichia coli*, *J Bacteriol* 171, 6555-6565.
13. Price, A. C., Zhang, Y. M., Rock, C. O., and White, S. W. (2001) Structure of beta-ketoacyl-[acyl carrier protein] reductase from *Escherichia coli*: negative cooperativity and its structural basis, *Biochemistry* 40, 12772-12781.
14. Price, A. C., Zhang, Y. M., Rock, C. O., and White, S. W. (2004) Cofactor-induced conformational rearrangements establish a catalytically competent active site and a proton relay conduit in FabG, *Structure* 12, 417-428.
15. Heath, R. J., and Rock, C. O. (1995) Enoyl-acyl carrier protein reductase (fabI) plays a determinant role in completing cycles of fatty acid elongation in *Escherichia coli*, *J Biol Chem* 270, 26538-26542.
16. Baldock, C., Rafferty, J. B., Sedelnikova, S. E., Baker, P. J., Stuitje, A. R., Slabas, A. R., Hawkes, T. R., and Rice, D. W. (1996) A mechanism of drug action revealed by structural studies of enoyl reductase, *Science* 274, 2107-2110.
17. Baldock, C., de Boer, G. J., Rafferty, J. B., Stuitje, A. R., and Rice, D. W. (1998) Mechanism of action of diazaborines, *Biochem Pharmacol* 55, 1541-1549.
18. Grassberger, M. A., Turnowsky, F., and Hildebrandt, J. (1984) Preparation and antibacterial activities of new 1,2,3-diazaborine derivatives and analogues, *J Med Chem* 27, 947-953.

19. Quemard, A., Sacchettini, J. C., Dessen, A., Vilcheze, C., Bittman, R., Jacobs, W. R., Jr., and Blanchard, J. S. (1995) Enzymatic characterization of the target for isoniazid in *Mycobacterium tuberculosis*, *Biochemistry* 34, 8235-8241.
20. Rozwarski, D. A., Grant, G. A., Barton, D. H., Jacobs, W. R., Jr., and Sacchettini, J. C. (1998) Modification of the NADH of the isoniazid target (InhA) from *Mycobacterium tuberculosis*, *Science* 279, 98-102.
21. Ramaswamy, S. V., Reich, R., Dou, S. J., Jasperse, L., Pan, X., Wanger, A., Quitugua, T., and Graviss, E. A. (2003) Single nucleotide polymorphisms in genes associated with isoniazid resistance in *Mycobacterium tuberculosis*, *Antimicrob Agents Chemother* 47, 1241-1250.
22. Sivaraman, S., Sullivan, T. J., Johnson, F., Novichenok, P., Cui, G., Simmerling, C., and Tonge, P. J. (2004) Inhibition of the bacterial enoyl reductase FabI by triclosan: a structure-reactivity analysis of FabI inhibition by triclosan analogues, *J Med Chem* 47, 509-518.
23. Sullivan, T. J., Truglio, J. J., Boyne, M. E., Novichenok, P., Zhang, X., Stratton, C. F., Li, H. J., Kaur, T., Amin, A., Johnson, F., Slayden, R. A., Kisker, C., and Tonge, P. J. (2006) High affinity InhA inhibitors with activity against drug-resistant strains of *Mycobacterium tuberculosis*, *ACS Chem Biol* 1, 43-53.
24. Rafi, S. B., Cui, G., Song, K., Cheng, X., Tonge, P. J., and Simmerling, C. (2006) Insight through molecular mechanics Poisson-Boltzmann surface area calculations into the binding affinity of triclosan and three analogues for FabI, the *E. coli* enoyl reductase, *J Med Chem* 49, 4574-4580.

25. Freundlich, J. S., Wang, F., Tsai, H. C., Kuo, M., Shieh, H. M., Anderson, J. W., Nkrumah, L. J., Valderramos, J. C., Yu, M., Kumar, T. R., Valderramos, S. G., Jacobs, W. R., Jr., Schiehser, G. A., Jacobus, D. P., Fidock, D. A., and Sacchettini, J. C. (2007) X-ray structural analysis of Plasmodium falciparum enoyl acyl carrier protein reductase as a pathway toward the optimization of triclosan antimalarial efficacy, *J Biol Chem* 282, 25436-25444.
26. Stewart, M. J., Parikh, S., Xiao, G., Tonge, P. J., and Kisker, C. (1999) Structural basis and mechanism of enoyl reductase inhibition by triclosan, *J Mol Biol* 290, 859-865.
27. Luckner, S. R., Liu, N., am Ende, C. W., Tonge, P. J., and Kisker, C. (2010) A slow, tight binding inhibitor of InhA, the enoyl-acyl carrier protein reductase from Mycobacterium tuberculosis, *J Biol Chem* 285, 14330-14337.
28. Wang, L. Q., Falany, C. N., and James, M. O. (2004) Triclosan as a substrate and inhibitor of 3'-phosphoadenosine 5'-phosphosulfate-sulfotransferase and UDP-glucuronosyl transferase in human liver fractions, *Drug Metab Dispos* 32, 1162-1169.
29. Yum, J. H., Kim, C. K., Yong, D., Lee, K., Chong, Y., Kim, C. M., Kim, J. M., Ro, S., and Cho, J. M. (2007) In vitro activities of CG400549, a novel FabI inhibitor, against recently isolated clinical staphylococcal strains in Korea, *Antimicrob Agents Chemother* 51, 2591-2593.
30. (1984) Classics in infectious diseases. "On abscesses". Alexander Ogston (1844-1929), *Rev Infect Dis* 6, 122-128.
31. (1998) Revised guidelines for the control of methicillin-resistant Staphylococcus aureus infection in hospitals. British Society for Antimicrobial Chemotherapy, Hospital

- Infection Society and the Infection Control Nurses Association, *J Hosp Infect* 39, 253-290.
32. Bamber, A. I., and Neal, T. J. (1999) An assessment of triclosan susceptibility in methicillin-resistant and methicillin-sensitive *Staphylococcus aureus*, *J Hosp Infect* 41, 107-109.
 33. Schiebel, J., Chang, A., Lu, H., Baxter, M. V., Tonge, P. J., and Kisker, C. (2012) *Staphylococcus aureus* FabI: inhibition, substrate recognition, and potential implications for in vivo essentiality, *Structure* 20, 802-813.
 34. Tipparaju, S. K., Joyasawal, S., Forrester, S., Mulhearn, D. C., Pegan, S., Johnson, M. E., Mesecar, A. D., and Kozikowski, A. P. (2008) Design and synthesis of 2-pyridones as novel inhibitors of the *Bacillus anthracis* enoyl-ACP reductase, *Bioorg Med Chem Lett* 18, 3565-3569.
 35. Chaturvedi, P. R., Decker, C. J., and Odinecs, A. (2001) Prediction of pharmacokinetic properties using experimental approaches during early drug discovery, *Curr Opin Chem Biol* 5, 452-463.
 36. Veber, D. F., Johnson, S. R., Cheng, H. Y., Smith, B. R., Ward, K. W., and Kopple, K. D. (2002) Molecular properties that influence the oral bioavailability of drug candidates, *J Med Chem* 45, 2615-2623.
 37. Lipinski, C. A., Lombardo, F., Dominy, B. W., and Feeney, P. J. (1997) Experimental and computational approaches to estimate solubility and permeability in drug discovery and development settings, *Adv Drug Deliver Rev* 23, 3-25.

38. Lipinski, C. A., Lombardo, F., Dominy, B. W., and Feeney, P. J. (2001) Experimental and computational approaches to estimate solubility and permeability in drug discovery and development settings, *Adv Drug Deliv Rev* 46, 3-26.
39. Perry, R. D., and Fetherston, J. D. (1997) *Yersinia pestis*--etiologic agent of plague, *Clin Microbiol Rev* 10, 35-66.
40. Ayyadurai, S., Sebbane, F., Raoult, D., and Drancourt, M. (2010) Body lice, *Yersinia pestis* orientalis, and black death, *Emerg Infect Dis* 16, 892-893.
41. Inglesby, T. V., Dennis, D. T., Henderson, D. A., Bartlett, J. G., Ascher, M. S., Eitzen, E., Fine, A. D., Friedlander, A. M., Hauer, J., Koerner, J. F., Layton, M., McDade, J., Osterholm, M. T., O'Toole, T., Parker, G., Perl, T. M., Russell, P. K., Schoch-Spana, M., and Tonat, K. (2000) Plague as a biological weapon: medical and public health management. Working Group on Civilian Biodefense, *JAMA* 283, 2281-2290.
42. Prentice, M. B., and Rahalison, L. (2007) Plague, *Lancet* 369, 1196-1207.
43. Reichert, J. M. (2001) Monoclonal antibodies in the clinic, *Nat Biotechnol* 19, 819-822.
44. Heath, R. J., and Rock, C. O. (2004) Fatty acid biosynthesis as a target for novel antibacterials, *Curr Opin Investig Drugs* 5, 146-153.
45. Massengo-Tiasse, R. P., and Cronan, J. E. (2008) *Vibrio cholerae* FabV defines a new class of enoyl-acyl carrier protein reductase, *J Biol Chem* 283, 1308-1316.
46. Massengo-Tiasse, R. P., and Cronan, J. E. (2009) Diversity in enoyl-acyl carrier protein reductases, *Cell Mol Life Sci* 66, 1507-1517.
47. Lu, H., and Tonge, P. J. (2010) Mechanism and inhibition of the FabV enoyl-ACP reductase from *Burkholderia mallei*, *Biochemistry* 49, 1281-1289.

48. Hirschbeck, M. W., Kuper, J., Lu, H., Liu, N., Neckles, C., Shah, S., Wagner, S., Sotriffer, C. A., Tonge, P. J., and Kisker, C. (2012) Structure of the *Yersinia pestis* FabV enoyl-ACP reductase and its interaction with two 2-pyridone inhibitors, *Structure* 20, 89-100.
49. Meena, L. S., and Rajni. (2010) Survival mechanisms of pathogenic *Mycobacterium tuberculosis* H37Rv, *FEBS J* 277, 2416-2427.
50. Blanchard, J. S. (1996) Molecular mechanisms of drug resistance in *Mycobacterium tuberculosis*, *Annual Review of Biochemistry* 65, 215-239.
51. Oliveira, J. S., de Sousa, E. H., de Souza, O. N., Moreira, I. S., Santos, D. S., and Basso, L. A. (2006) Slow-onset inhibition of 2-trans-enoyl-ACP (CoA) reductase from *Mycobacterium tuberculosis* by an inorganic complex, *Curr Pharm Des* 12, 2409-2424.
52. Tonge, P. J. (2000) Another brick in the wall, *Nat Struct Biol* 7, 94-96.
53. Lu, H., and Tonge, P. J. (2010) Drug-target residence time: critical information for lead optimization, *Curr Opin Chem Biol* 14, 467-474.
54. Chhibber, M., Kumar, G., Parasuraman, P., Ramya, T. N., Surolia, N., and Surolia, A. (2006) Novel diphenyl ethers: design, docking studies, synthesis and inhibition of enoyl ACP reductase of *Plasmodium falciparum* and *Escherichia coli*, *Bioorg Med Chem* 14, 8086-8098.
55. Min C. K., L. Y. H., Kyu D. S., Seonggu R., Myung J. C. . (2007) Heterocycles, particularly 1,4-disubstituted 1H-pyridin-2-ones, processes for preparing them, pharmaceutical compositions containing them, and their use as Fab I (NADH-dependent enoyl-ACP reductase) inhibitors, *PCT Int. Appl.*, 119.

56. Parikh, S. L., Xiao, G., and Tonge, P. J. (2000) Inhibition of InhA, the enoyl reductase from *Mycobacterium tuberculosis*, by triclosan and isoniazid, *Biochemistry* 39, 7645-7650.
57. Xu, H., Sullivan, T. J., Sekiguchi, J., Kirikae, T., Ojima, I., Stratton, C. F., Mao, W., Rock, F. L., Alley, M. R., Johnson, F., Walker, S. G., and Tonge, P. J. (2008) Mechanism and inhibition of saFabI, the enoyl reductase from *Staphylococcus aureus*, *Biochemistry* 47, 4228-4236.